



Five years of CO, HCN, C₂H₆, C₂H₂, CH₃OH, HCOOH and H₂CO total columns measured in the Canadian high Arctic

C. Viatte¹, K. Strong¹, K. A. Walker^{1,2}, and J. R. Drummond^{1,3}

¹Department of Physics, University of Toronto, Toronto, Ontario, Canada

²Department of Chemistry, University of Waterloo, Ontario, Canada

³Department of Physics and Atmospheric Sciences, Dalhousie University, Halifax, Canada

Correspondence to: C. Viatte (viatte@atmosph.physics.utoronto.ca)

Received: 9 October 2013 – Published in Atmos. Meas. Tech. Discuss.: 20 December 2013

Revised: 14 April 2014 – Accepted: 21 April 2014 – Published: 3 June 2014

Abstract. We present a five-year time series of seven tropospheric species measured using a ground-based Fourier transform infrared (FTIR) spectrometer at the Polar Environment Atmospheric Research Laboratory (PEARL; Eureka, Nunavut, Canada; 80°05' N, 86°42' W) from 2007 to 2011. Total columns and temporal variabilities of carbon monoxide (CO), hydrogen cyanide (HCN) and ethane (C₂H₆) as well as the first derived total columns at Eureka of acetylene (C₂H₂), methanol (CH₃OH), formic acid (HCOOH) and formaldehyde (H₂CO) are investigated, providing a new data set in the sparsely sampled high latitudes.

Total columns are obtained using the SFIT2 retrieval algorithm based on the optimal estimation method. The microwindows as well as the a priori profiles and variabilities are selected to optimize the information content of the retrievals, and error analyses are performed for all seven species. Our retrievals show good sensitivities in the troposphere. The seasonal amplitudes of the time series, ranging from 34 to 104 %, are captured while using a single a priori profile for each species. The time series of the CO, C₂H₆ and C₂H₂ total columns at PEARL exhibit strong seasonal cycles with maxima in winter and minima in summer, in opposite phase to the HCN, CH₃OH, HCOOH and H₂CO time series. These cycles result from the relative contributions of the photochemistry, oxidation and transport as well as biogenic and biomass burning emissions.

Comparisons of the FTIR partial columns with coincident satellite measurements by the Atmospheric Chemistry Experiment Fourier Transform Spectrometer (ACE-FTS) show good agreement. The correlation coefficients and the slopes

range from 0.56 to 0.97 and 0.50 to 3.35, respectively, for the seven target species.

Our new data set is compared to previous measurements found in the literature to assess atmospheric budgets of these tropospheric species in the high Arctic. The CO and C₂H₆ concentrations are consistent with negative trends observed over the Northern Hemisphere, attributed to fossil fuel emission decrease. The importance of poleward transport for the atmospheric budgets of HCN and C₂H₂ is highlighted. Columns and variabilities of CH₃OH and HCOOH at PEARL are comparable to previous measurements performed at other remote sites. However, the small columns of H₂CO in early May might reflect its large atmospheric variability and/or the effect of the updated spectroscopic parameters used in our retrievals. Overall, emissions from biomass burning contribute to the day-to-day variabilities of the seven tropospheric species observed at Eureka.

1 Introduction

Future climate change may cause significant reduction in air quality by changing the outflow of pollutants as well as the strength of emissions from the biosphere, fires and dust. The sign and magnitude of these effects are highly uncertain and will vary regionally (IPCC, 2007). This is especially true in sensitive areas, such as the Arctic, which has been warming rapidly over the past century (Trenberth et al., 2007; Lesins et al., 2010). The chemical environment of the Arctic is unique and characterized by low temperatures, extremes in radiation

Table 1. Sources, sinks and average lifetimes of all the target species. BB, VOC and NMHCs are the acronyms of biomass burning, volatile organic compound and non-methane hydrocarbons, respectively.

Target species	Name	Sources	Sinks	Lifetimes
CO	Carbon monoxide	BB, transport, steel industry, methane and VOC oxidation	Reaction with OH	2 months
HCN	Hydrogen cyanide	BB, industry, fungi and plant emission	Reaction with OH and ocean uptake	2–6 months
C ₂ H ₆	Ethane	BB, biofuel use, natural emission	Reaction with OH	1.5 months
C ₂ H ₂	Acetylene	BB, combustion product, natural emission	Reaction with OH	2 weeks
CH ₃ OH	Methanol	BB, biogenic emission	Reaction with OH	5–10 days
HCOOH	Formic acid	BB, biogenic emission, photo-oxidation of NMHCs	Reaction with OH, dry and wet deposition	3–4 days
H ₂ CO	Formaldehyde	BB, oxidation of methane and NMHCs	Reaction with OH	< 2 days

with long periods of light and darkness, and chemical processes involving snow and ice at the surface. The Arctic is a major receptor for mid-latitude pollution (Shaw, 1995; Quinn et al., 2007, 2008) and changes in chemistry and influx of pollution may disrupt this sensitive system (Rinke et al., 2004). Several studies have identified pollution transport to the Arctic based on model simulations and meteorological analyses (Eckhardt et al., 2003; Klonecki et al., 2003; Koch and Hansen, 2005; Stohl, 2006; Shindell et al., 2008), but our ability to verify these pathways through chemical observations has been limited.

Ground-based solar absorption spectroscopy can be used to measure atmospheric composition for the validation of satellite remote-sensing instruments and model data. The variability of tropospheric trace gases in remote areas can be quantified using long-term monitoring of molecules released by both natural sources and human activities. This contributes to a better understanding of Arctic chemistry as well as the factors driving current changes in Arctic atmospheric composition and climate. In this study, we investigate the atmospheric concentrations and variabilities of seven tropospheric trace gases using ground-based Fourier transform infrared (FTIR) spectra, recorded at the Polar Environment Atmospheric Research Laboratory (PEARL; Eureka, Nunavut, Canada; 80°05' N, 86°42' W) from 2007 to 2011. These molecules (listed in Table 1) are carbon monoxide (CO), hydrogen cyanide (HCN), ethane (C₂H₆), acetylene (C₂H₂), methanol (CH₃OH), formic acid (HCOOH) and formaldehyde (H₂CO). They have different source and sink mechanisms and their different lifetimes play a role in their observed seasonal variabilities (Notholt et al., 1997a).

CO, HCN, C₂H₆ and C₂H₂ total and partial columns have been measured by ground-based FTIR spectroscopy at several locations in the Northern Hemisphere (Mahieu et al.,

1997; Rinsland et al., 1998, 2000; Zhao et al., 2002) and in the Southern Hemisphere (Rinsland et al., 1999, 2001, 2002; Paton-Walsh et al., 2010; Vigouroux et al., 2012). CH₃OH and HCOOH have been measured in a limited number of ground-based FTIR studies (Paton-Walsh et al., 2005, 2008; Rinsland et al., 2004, 2009; Zander et al., 2010; Paulot et al., 2011). The first FTIR data sets of H₂CO were obtained in remote areas (Mahieu et al., 1997; Notholt et al., 1997a, b) and were then extended to urban areas (Hak et al., 2005) and the Southern Hemisphere (Jones et al., 2009; Vigouroux et al., 2009; Paton-Walsh et al., 2010).

In the Arctic, remote measurements of these tropospheric species have been performed using ground-based, aircraft and satellite platforms. For instance, the Infrared Atmospheric Sounding Interferometer (IASI) has measured CH₃OH and HCOOH globally from space, but no observations are available above 45° N in winter and 65° N in summer, because of the thermal emission sensitivity of this instrument (Razavi et al., 2011). The Michelson Interferometer for Passive Atmospheric Sounding (MIPAS) limb emission instrument mapped upper-tropospheric distributions of several species, such as HCN and C₂H₆ (Glatthor et al., 2009). It also measured HCOOH at a 10 km altitude between 70 and 90° N (Grutter et al., 2010). The Atmospheric Chemistry Experiment (ACE) is able to monitor all seven species derived in this study, with periodic sampling over the Arctic. It has been used to measure CO, C₂H₆, HCN, C₂H₂, CH₃OH and HCOOH in the upper troposphere over Alaska and Canada (Rinsland et al., 2007) as well as H₂CO over North America (50–80° N) (Dufour et al., 2009).

Furthermore, several campaigns have investigated the atmospheric composition of the Arctic including the Polar Study using Aircraft, Remote Sensing, Surface Measurements and Models, of Climate, Chemistry, Aerosols, and

Transport (POLARCAT, http://www.atmos-chem-phys.net/special_issue182.html) and the Arctic Research of the Composition of the Troposphere from Aircraft and Satellites (ARCTAS; Jacob et al., 2010). During these campaigns, several aircraft measurements of the target species, listed in Table 1, were reported in biomass burning plumes (Goode et al., 2000; Simpson et al., 2011; Le Breton et al., 2013).

In contrast to these measurements, the ground-based FTIR technique can provide total columns, with good sensitivity in the lower troposphere (compared to satellite measurements), as well as long-term spectral acquisition, in clear-sky conditions, thereby enabling an assessment of the temporal variabilities of the target species in the high Arctic (compared to campaign-based measurements). We focused on these species because there remain numerous gaps in the available observational data sets, especially at high latitudes. Furthermore, the transport and the degradation mechanisms of non-methane hydrocarbons (NMHCs) are poorly understood and should be better quantified in order to increase our ability to predict trace gas concentrations and variability in models (Stavrakou et al., 2009).

For instance, simulated CO concentrations disagreed by a factor of two to three at all altitudes in the Arctic in a comparison of eleven chemical transport models (Shindell et al., 2008). This has been attributed to model differences in emissions, transport and OH concentrations. Thus, there is a need to better understand the sources and the transport of CO to the Arctic, as an indicator of pollution effects (Fisher et al., 2010). Concerning C₂H₂, large uncertainties remain with regard to the magnitude of its sources and sinks as well as its spatial distribution and seasonality in the atmosphere (Parker et al., 2011). In addition, large uncertainties remain in the CH₃OH atmospheric budget in terms of its source magnitudes, seasonality and spatial distribution in the atmosphere (Millet et al., 2008). Concerning HCOOH, several studies have highlighted the underestimation of emissions in the models by a factor of nine in the marine boundary layer (Baboukas et al., 2000) and an order of magnitude for the free troposphere (Von Kuhlmann et al., 2003). Recently, Paulot et al. (2011) investigated an underestimation in the model by a factor of two to five compared to polar FTIR measurements at Thule (Greenland; 76° N, 69° W), confirming the missing local sources in the HCOOH budget simulated in the model. Finally, HCOOH and H₂CO spectroscopic parameters have been refined recently (HITRAN 2008, <http://www.cfa.harvard.edu/hitran/updates.html>, Rothman et al., 2009). These improvements increase the HCOOH infrared band intensity by a factor of two (Perrin and Vander Auwera, 2007) and increase the H₂CO line intensities by about 30 % in the spectral region of 3.6 microns (Perrin et al., 2009), used in this study. It is thus important to generate new data sets with improved spectroscopic parameters and optimized retrievals to help improve atmospheric model simulations and expand our knowledge about the chemical and dynamical processes of the high Arctic.

This paper first describes the methodology employed to obtain our data set. The FTIR measurements and retrievals are presented for each of the seven tropospheric species, CO, HCN, C₂H₆, C₂H₂, CH₃OH, HCOOH and H₂CO, observed at Eureka from 2007 to 2011. Details about the selected microwindows, a priori information, information content of the retrievals and error analyses are described in Sect. 2. This section also describes the procedure employed to compare our data set with the ACE-FTS (Atmospheric Chemistry Experiment Fourier Transform Spectrometer) satellite measurements. In Sect. 3, the time series are discussed in terms of their seasonal variabilities in connection with the different origins and atmospheric lifetimes of the molecules. Results of the comparisons between our data set and the ACE-FTS and previous measurements reported in the literature are presented. This leads to a discussion of the atmospheric budget of the different target species observed in the high Arctic.

2 Methodology

2.1 FTIR measurements at PEARL

We present five years of observations of seven tropospheric species, listed in Table 1, from 2007 to 2011. These time series are obtained from ground-based FTIR measurements made in the high Arctic at PEARL (80°05' N, 86°42' W, 0.61 km a.s.l.; Eureka, Nunavut, Canada; Fogal et al., 2013). This high-resolution solar absorption spectrometer (Bruker IFS 125HR, operated at a maximum optical path difference = 257 cm) is part of the international Network for the Detection of Atmospheric Composition Change (NDACC, <http://www.ndsc.ncep.noaa.gov/>). It was installed at PEARL by the Canadian Network for the Detection of Atmospheric Change (CANDAC) in July 2006 (Batchelor et al., 2009; Lindenmaier, 2012). The spectrometer measures spectra using two detectors (indium antimonide – InSb – or mercury cadmium telluride – MCT), a potassium bromide (KBr) beam splitter and a sequence of seven narrow-band interference filters covering the 600–4300 cm⁻¹ spectral range. No apodization is applied to these measurements. A reference low-pressure hydrogen bromide (HBr) cell spectrum is recorded regularly with the internal globar to characterize the instrumental line shape (ILS) and monitor the alignment of the instrument. By using the LINEFIT software analysis (Hase et al., 1999), the modulation efficiency and the phase error are retrieved and included in the forward model.

As we are using an NDACC instrument, CO, HCN and C₂H₆ are retrieved following the InfraRed Working Group (IRWG, <http://www.acd.ucar.edu/irwg/>) recommendations. For the other species, C₂H₂, CH₃OH, HCOOH and H₂CO, the full retrieval methodology was developed in this work. The CH₃OH total columns shown here are the first retrieved from ground-based FTIR measurements in the high Arctic. Total columns of CO, HCN and C₂H₆ were recently used

to investigate the composition of an intense biomass burning plume transported from Russia to Eureka in August 2010 (Viatte et al., 2013).

Total columns of CO, HCN, C₂H₆, C₂H₂, CH₃OH, HCOOH and H₂CO result from the analysis of 3980, 1815, 1819, 1269, 1095, 1973 and 1242 spectra, respectively, recorded between 2007 and 2011. Because solar absorption FTIR measurements require the sun as the source, there are no data from mid-October to mid-February (polar night). Thus, the time series are from February to October for CO, HCN, C₂H₂ and HCOOH, from March to October for C₂H₆ and H₂CO and from March to September for CH₃OH. The differences in the number of observations and the duration of the time series are the results of the quality filter used to reject inconsistent retrievals. They are based on negative volume mixing ratio (VMR) values (due to small oscillations in the retrieval), root mean square (rms) residuals exceeding a threshold value (of two average standard deviations from the median of all rms residuals) and failure to converge after fifteen iterations in the inversion procedure.

2.2 Microwindows

Atmospheric trace gas concentrations are retrieved using inversion procedures performed on atmospheric spectra, within suitable spectral regions, called microwindows. The choice of microwindows (MWs) is crucial because the majority of the target species have relatively weak absorptions in the infrared region compared to the main interfering species, such as CH₄, H₂O and O₃. All MWs have been selected in order to increase the information content and minimize the errors in the retrievals. These MWs are shown in Figs. 1 and 2, with examples of spectra recorded in clear and polluted conditions given in blue and red, respectively. The MWs of CO and C₂H₆ were selected based on the recommendations of the NDACC/IRWG in their harmonization effort strategy.

The CO total columns are retrieved in three widely used MWs, including a weak line of CO at 2057.858 cm⁻¹, another weak line of CO at 2069.656 cm⁻¹ and a strong line of CO at 2158.300 cm⁻¹ (Notholt et al., 2000; Zhao et al., 2002). The use of a combination between weak and strong absorption lines increases the vertical sensitivity of the retrievals (Barret et al., 2003). Interfering species (CO₂, O₃, OCS, N₂O and H₂O) are simultaneously scaled from their a priori profiles during the inversions. In order to obtain a good estimate of the measurement noise covariance matrix, we constructed trade-off curves of the rms residual (i.e. spectral fit residuals of the retrieval) versus SNR (signal-to-noise ratio) (Batchelor et al., 2009). The resulting SNR of 85 minimized the rms residuals and maximized the DOFS (degrees of freedom for signal) of the CO retrievals.

For HCN, two MWs, around 3287.248 cm⁻¹ (Mahieu et al., 1997; Notholt et al., 2000; Zhao et al., 2002) and around 3268.200 cm⁻¹, are preferred over the three IRWG recommendations (which are 3268.05–3268.40, 3287.10–3287.35

and 3299.40–3299.60 cm⁻¹). This choice increases the information content and decreases the errors in the Eureka retrievals. The profiles of the only interfering species, H₂O, are scaled from the a priori profile and an SNR of 200 is used in the retrievals.

The C₂H₆ retrievals are performed in three MWs around 2976.800 cm⁻¹ (Mahieu et al., 1997; Rinsland et al., 2002; Paton-Walsh et al., 2010), 2983.300 cm⁻¹ (Meier et al., 2004) and 2986.700 cm⁻¹ (Notholt et al., 1997a), using an SNR of 250. Single scaling parameters are used for each of the interfering gases (H₂O and O₃).

For C₂H₂, we use three MWs, around 3250.500 cm⁻¹ (Petersen et al., 2008), 3255.200 cm⁻¹ (Mahieu et al., 2008) and 3305.400 cm⁻¹ (Mahieu et al., 2008; Paton-Walsh et al., 2010). H₂O and its main isotopologue (HDO) are scaled simultaneously from their a priori profiles. Because the infrared absorptions of the target gas are weak compared to the H₂O lines, a reduced SNR is employed in the spectral region with no C₂H₂ features. While an SNR of 200 is used over all the MWs, we apply an SNR of 50 between 3250.430 and 3250.550 cm⁻¹ and between 3255.180 and 3255.455 cm⁻¹, and an SNR of 75 from 3305.065 to 3305.350 cm⁻¹.

For CH₃OH, we use the two MWs employed by Bader et al. (2013). In this region, the CH₃OH band at 1033 cm⁻¹ represents around 1.5 % of the absorption, whereas the O₃ lines represent about 94 %. Thus, O₃ and its isotopologues (¹⁶O¹⁸O¹⁶O labelled O₃⁶⁸⁶, ¹⁶O¹⁶O¹⁸O labelled O₃⁶⁶⁸, ¹⁶O¹⁷O¹⁶O labelled O₃⁶⁷⁶, and ¹⁶O¹⁶O¹⁷O labelled O₃⁶⁶⁷; Table 2) as well as the other interfering species (CO₂ and H₂O) are retrieved simultaneously by scaling their a priori profiles. We use an SNR of 200. For more clarity in Fig. 2, we show an example of spectral fitting with the contributions of all the species in the second MW. The significant broad absorption feature of CH₃OH can be seen from around 1032 to 1035 cm⁻¹ (Fig. 2, right-hand panel, cyan line).

For HCOOH, we use one MW between 1104.650 and 1105.600 cm⁻¹, which corresponds to the band used in Zander et al. (2010), Paulot et al. (2011) and Vigouroux et al. (2012). The spectroscopic parameters of this band have been updated (Perrin and Vander Auwera, 2007). Zander et al. (2010) have shown that these improvements reduce the retrieved total columns by a factor of two. In this MW, a global SNR of 800 is used and interfering species (HDO, O₃, O₃⁶⁶⁸, O₃⁶⁷⁶, H₂O, NH₃, CCl₂F₂, CHF₂Cl, CH₄) are simultaneously scaled from their a priori profiles.

For H₂CO, MWs are from Paton-Walsh et al. (2005) where the lines belong to two bands, centred at 2782.000 and 2843.000 cm⁻¹, respectively. The interfering species, such as CH₄, O₃, CO₂ and N₂O, are simultaneously scaled from their a priori profiles. The SNR assumed in the MWs is 500 and is reduced to 100 in the spectral regions where systematic residual features were caused by various inaccuracies in the CH₄ line parameters (Sussmann et al., 2011).

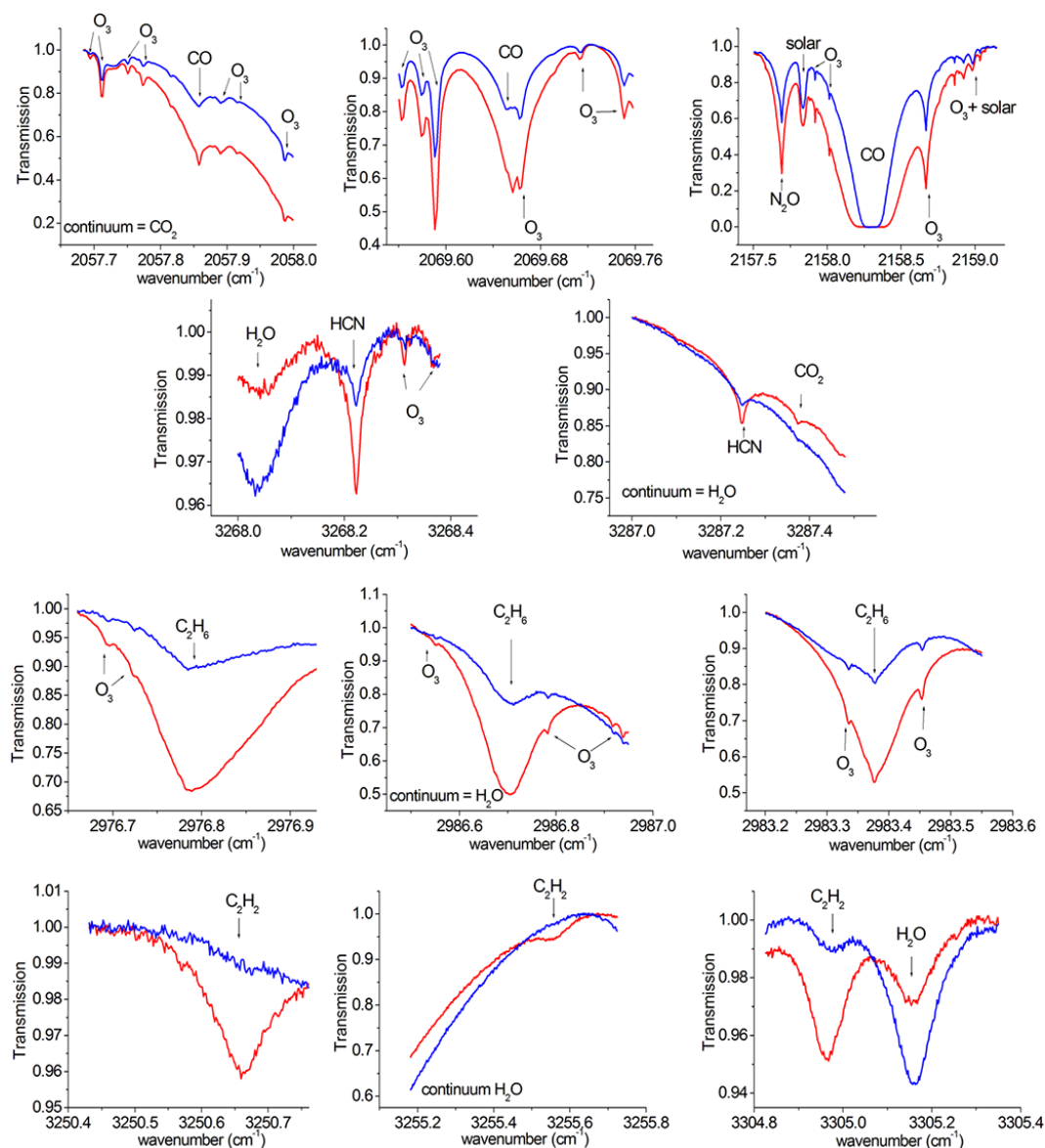


Figure 1. Microwindows used in the retrievals of CO, HCN, C₂H₆ and C₂H₂, with examples of clear and polluted conditions in blue and red, respectively.

2.3 Retrieval methodology: optimal estimation method

In order to retrieve atmospheric concentrations from the measured spectra, we use the SFIT2 algorithm (Pougatchev et al., 1995; Rinsland et al., 1998) version 3.94, which is based on a semi-empirical implementation of the optimal estimation method (OEM) of Rodgers (2000).

The inversion procedure is an ill-posed problem and requires the use of constraints to stabilize the solution, usually provided by the a priori information. This a priori knowledge is defined by the states of the atmosphere in terms of VMR vertical profiles and variabilities, for each molecule involved in the analysis (target and interfering species). The

retrieval and the forward model, which involves a radiative transfer calculation, also require appropriate meteorological parameters as well as a discretized vertical model of the atmosphere. Daily pressure and temperature profiles are from the National Centers for Environment Prediction (NCEP, <http://www.ncep.noaa.gov/>) and combined with daily averages of morning (11:00 UTC) and afternoon (23:00 UTC) radiosonde measurements performed at Environment Canada's Eureka weather station. Our retrieved profiles are obtained on a 48-level altitude grid (from 0.61 to 120 km) and total columns are then derived by vertically integrating these profiles.

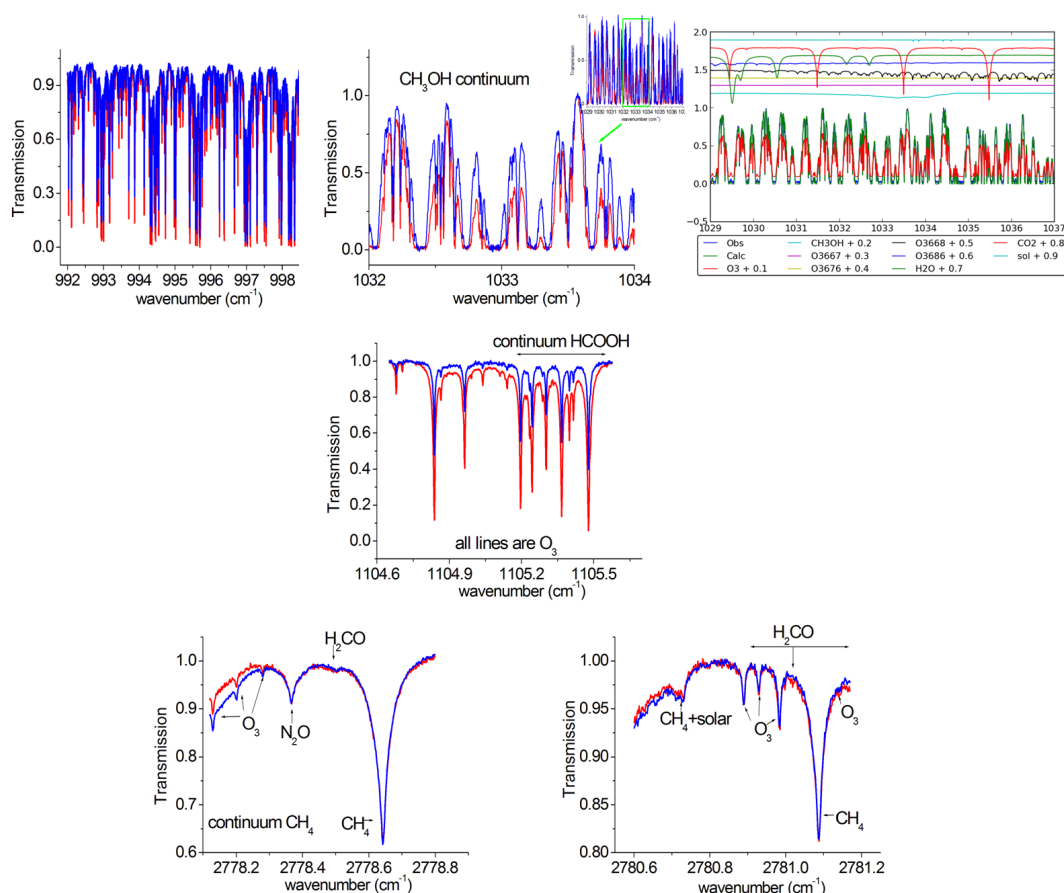


Figure 2. Microwindows used in the retrievals of CH₃OH, HCOOH and H₂CO, with examples of clear and polluted conditions in blue and red, respectively.

The vertical information content of the retrieved profiles is quantified by the DOFS, which corresponds to the trace of the averaging kernel matrix **A** (Rodgers, 2000), defined as

$$\mathbf{A} = \frac{\partial \hat{\mathbf{x}}}{\partial \mathbf{x}} = \left(\mathbf{K}^T \mathbf{S}_\varepsilon^{-1} \mathbf{K} + \mathbf{S}_a^{-1} \right)^{-1} \mathbf{K}^T \mathbf{S}_\varepsilon^{-1} \mathbf{K}, \quad (1)$$

where $\hat{\mathbf{x}}$ and \mathbf{x} represent the estimate and the true state vectors, respectively. **K** is the weighting function matrix that relates the measurement state to the true state of the atmosphere, **S**_ε is the measurement covariance matrix and **S**_a is the a priori covariance matrix used in the OEM.

The spectroscopic parameters are from the HITRAN 2008 database (Rothman et al., 2009) for all the species derived in this study. As noted in Sect. 1, it contains significant improvements concerning HCOOH and H₂CO line intensities in the spectral regions of interest.

The retrieval parameters (microwindows, interfering species, a priori VMR sources, diagonal values of the a priori covariance matrix and SNRs) used for all the target species are summarized in Table 2 and discussed below.

2.4 A priori information

The location of the instrument at high latitudes offers a relatively dry atmosphere (total precipitable water ranges between 0 and 1.8 g cm⁻²; Wagner et al., 2006, their Fig. 3). Compared to tropical FTIR sites, such as Reunion Island (Vigouroux et al., 2012) or Darwin in Australia (Paton-Walsh et al., 2010), our spectra are less affected by strong features due to water vapour abundance. Thus a pre-fitting of water vapour (or “two-step retrieval”) is not necessary here.

Instead, the difficulty resides in the lack of continuous tropospheric measurements in the Arctic, needed to build our a priori knowledge of the polar atmospheric states. Our a priori VMR profiles are from the Whole Atmosphere Community Climate Model (WACCM, <http://www2.cesm.ucar.edu/working-groups>) as recommended by the NDACC/IRWG, except for the C₂H₂ retrievals (see above). WACCM is a numerical model developed at the National Center for Atmospheric Research (Sassi et al., 2002) and is the model which was used to compute a 40-year average of the modelled profiles at Eureka, which served as a priori VMRs for the target species.

Table 2. Parameters (microwindows, interfering species, a priori VMR sources, standard deviations – SD – of the a priori covariance matrix and signal-to-noise ratios – SNR) used in the retrievals of the seven target gases.

Target species		Microwindows	Interfering species	A priori VMR	SD for S _a (%)	SNR
Carbon monoxide	CO	2057.684–2058.000, 2069.560–2069.760, 2157.507–2159.144	O ₃ , CO ₂ , OCS, H ₂ O, N ₂ O	WACCM v6	20	85
Hydrogen cyanide	HCN	3268.000–3268.380, 3287.000–3287.480	H ₂ O	WACCM v6	50	200
Ethane	C ₂ H ₆	2976.660–2976.950, 2983.200–2983.550, 2986.500–2986.950	H ₂ O, O ₃	WACCM v4.5	30	250
Acetylene	C ₂ H ₂	3250.430–3250.770, 3255.180–3255.725, 3304.825–3305.350	H ₂ O, HDO	GC Toon Kiruna991203 Mk4-flight 6–34 km, outside spitprim.set, divided by 2	50	200
Methanol	CH ₃ OH	992.000–998.700, 1029.000–1037.000	O ₃ , O ₃ ⁶⁸⁶ , O ₃ ⁶⁶⁸ , O ₃ ⁶⁷⁶ , O ₃ ⁶⁶⁷ , H ₂ O, CO ₂	WACCM v6	20	200
Formic acid	HCOOH	1104.650–1105.600	HDO, O ₃ , O ₃ ⁶⁶⁸ , O ₃ ⁶⁷⁶ , H ₂ O, NH ₃ , CCL ₂ F ₂ , CHF ₂ CL, CH ₄	WACCM v6	100	800
Formaldehyde	H ₂ CO	2778.120–2778.800, 2780.600–2781.170	CH ₄ , CO ₂ , O ₃ , N ₂ O	WACCM v6 divided by 2	100	500

In Figs. 3 to 9 (upper panels), the a priori profiles adopted for the FTIR retrievals are shown in black, with the mean of all retrieved profiles in red. The black and red error bars correspond to the standard deviation of the a priori covariance matrix used in the retrievals and the standard deviations around the mean retrieved profiles, respectively, at each layer. All the a priori VMR profiles exhibit large contributions in the boundary layer and the troposphere, and decrease to almost zero at 50 km, except for CO, for which the sources are dominated by CH₄ oxidation at this altitude (Clerbaux et al., 2008).

The CO a priori VMR is about 92 ppbv (1 ppbv = 10^{−9} per unit volume) through the boundary layer, decreases to about 20 ppbv in the tropopause region and increases again with altitude to 0.6 ppmv (1 ppmv = 10^{−6} per unit volume) at 50 km. The HCN a priori VMR increases slightly from 25 to 32 ppbv in the troposphere and decreases in the stratosphere to reach 11 ppbv in the stratosphere. The C₂H₆, C₂H₂ and CH₃OH a priori VMR profiles have similar shapes as a function of altitude. Note that the C₂H₆ and C₂H₂ profiles are plotted on a log scale whereas the CH₃OH profile is plotted on a linear scale for clarity (Figs. 3 to 9, upper panels). Their VMRs are

almost constant in the boundary layer and the troposphere, with values of about 1 ppbv for C₂H₆ and 0.5 ppbv for both C₂H₂ and CH₃OH. At the upper altitudes, the a priori profiles of C₂H₆, C₂H₂ and CH₃OH decrease until reaching ~ 1 pptv (1 pptv = 10^{−12} per unit volume) at 22, 17 and 21 km, respectively. For HCOOH and H₂CO, the a priori VMRs in the boundary layer are about 8 and 30 pptv and then decrease to 1 and 10 pptv around 30 km for HCOOH and H₂CO, respectively. However, the sinks and sources are not as well understood (Paulot et al., 2011; Jones et al., 2009), especially in the polar region, so the interpretation of the a priori profiles has to be done carefully.

The a priori VMR profiles are from WACCM version 6 for CO, HCN, CH₃OH and HCOOH, and divided by two at all altitudes for H₂CO (see explanation below). The low stratospheric values of C₂H₆ VMRs in WACCM version 6 were beyond the retrieval software precision, therefore the a priori VMR profiles of C₂H₆ are from WACCM version 4.5. For C₂H₂, the a priori profile assumed here is not derived from WACCM because the VMR values were extremely low in the upper atmosphere and not representative, causing the retrievals to rarely converge. To avoid these instabilities in the

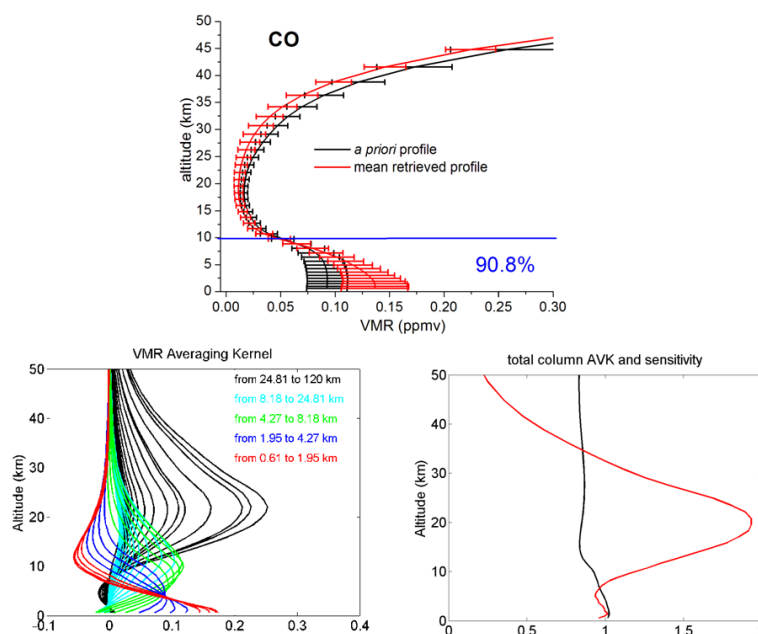


Figure 3. The CO a priori VMR profile from WACCM v6 in black (upper panel). The black error bars represent the standard deviation of the a priori covariance matrix used in the retrievals at each layer. The mean retrieved profile is in red, with error bars corresponding to the 1σ standard deviation from the mean. The number in blue is the percentages of the tropospheric column contributions (between 0.6 and 10.7 km) relative to the total column (between 0.6 and 120 km). Typical VMR averaging kernels in VMR/VMR (lower left panel), total-column Averaging kernels (AVK) in (molecule cm^{-2})/(molecule cm^{-2}) (lower right-hand panels, black line) and sensitivity profiles (right-hand panel, red line) as a function of altitude. The colours correspond to averaging kernels at altitudes lying in a partial column for which the DOFS is about 0.5.

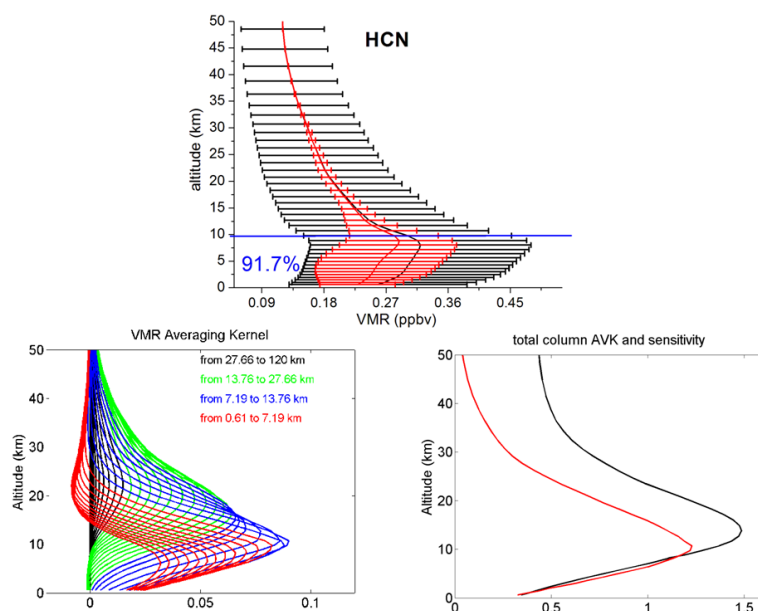


Figure 4. Same as Fig. 3 but for HCN.

retrievals, we used a profile derived from MkIV balloon measurements made at the high-latitude NDACC site of Kiruna (Sweden; Toon et al., 1999), at between 6 and 34 km altitude, combined with spitprim.set (Ft. Sumner MkIV flights, 1990s,

<http://mark4sun.jpl.nasa.gov/m4.html>). This a priori profile has been divided by two so that the tropospheric VMR values are comparable to the ones derived from the WACCM runs.

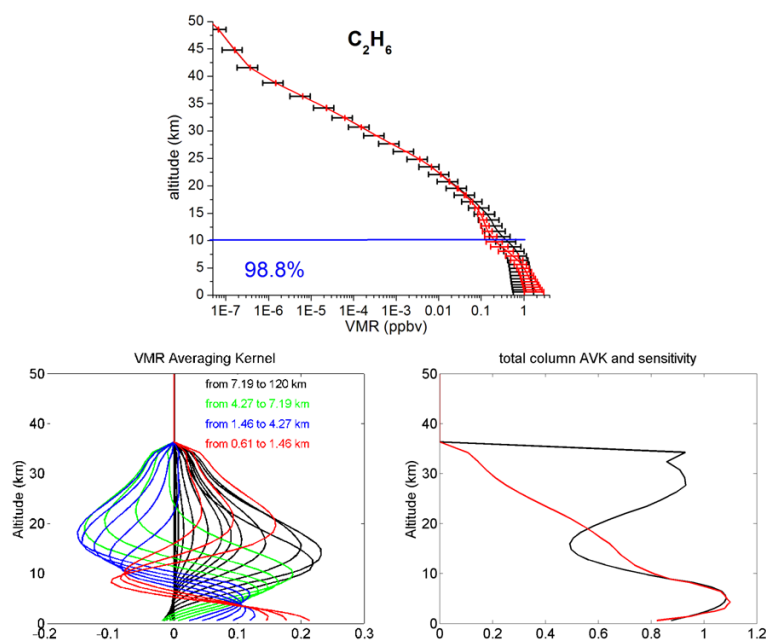


Figure 5. Same as Fig. 3 but for C₂H₆. The C₂H₆ a priori VMR profile is from WACCM v4.5.

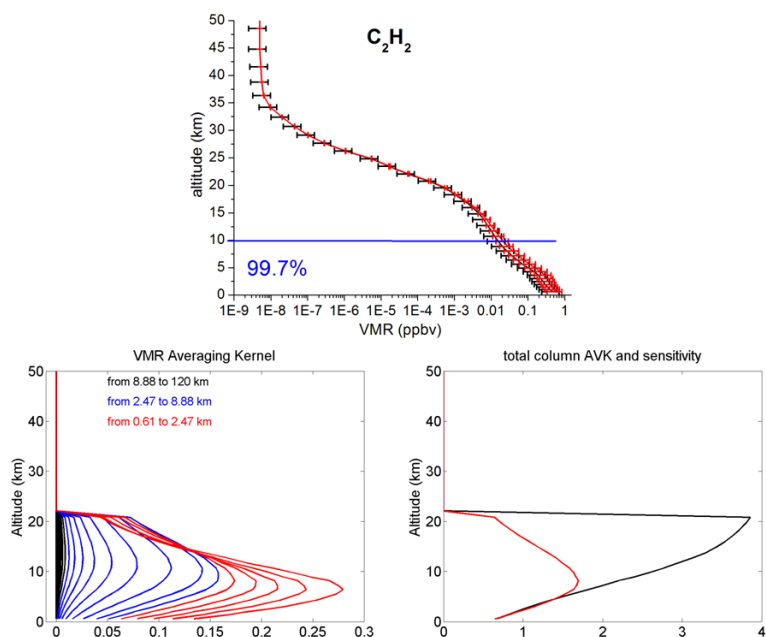


Figure 6. Same as Fig. 3 but for C₂H₂. The C₂H₂ a priori VMR profile is from MkIV balloon measurements made at the high-latitude NDACC site of Kiruna, at between 6 and 34 km altitude, combined with spitprim.set (Ft. Sumner MkIV flights, 1990s, <http://mark4sun.jpl.nasa.gov/m4.html>).

Instabilities in the retrieval also appear if the measured columns are substantially smaller than the a priori columns. As a result, the retrieved profile returns non-physical negative mixing ratios at the altitudes where the information content is low. This means that the most practical approach is often to use a priori profiles with a significantly lower total column

than the average expected from the data set and to compensate by using larger values in the covariance matrix S_a (Paton-Walsh, 2009). Thus, the a priori profile of H₂CO has been divided by two in order to reduce the rms residual and avoid oscillations in the retrieved profiles. We also verified that the retrieved total columns did not change significantly

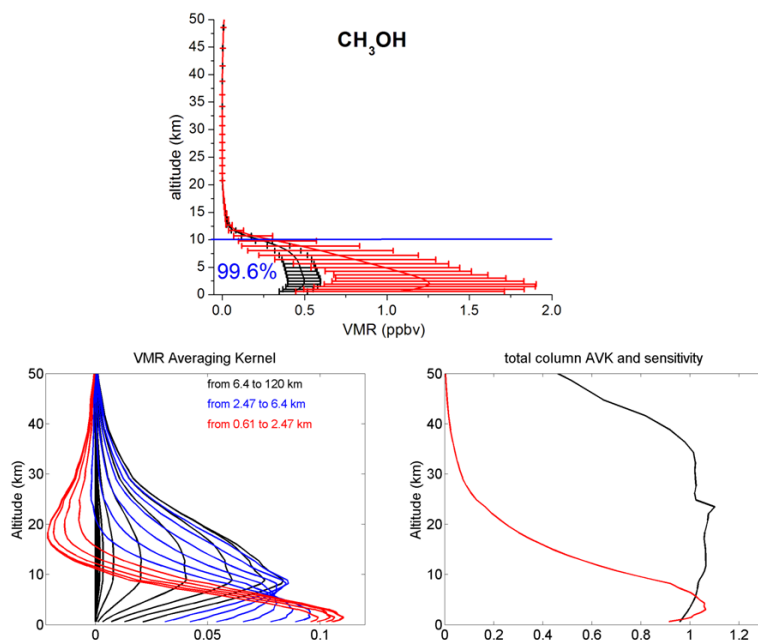


Figure 7. Same as Fig. 3 but for CH₃OH.

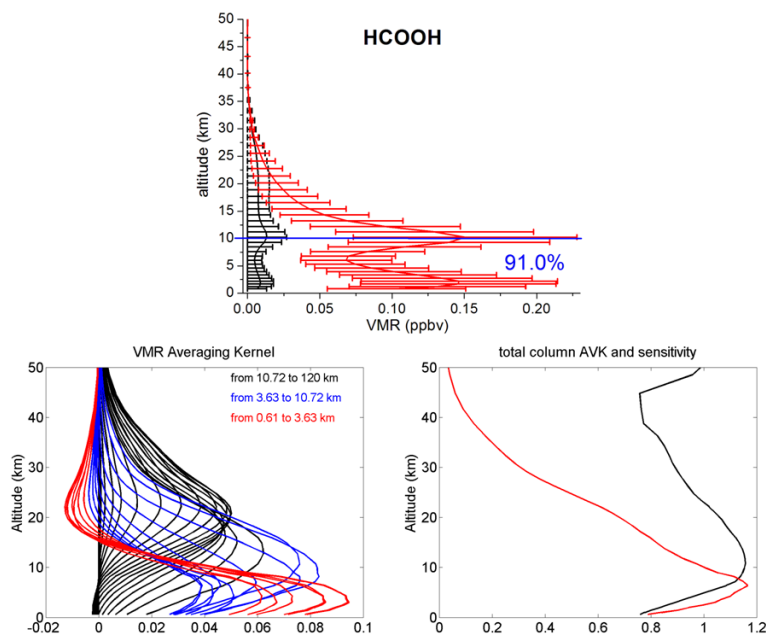


Figure 8. Same as Fig. 3 but for HCOOH.

(within error bars of the measurements) when using both profiles (that divided by two and that not divided). This confirms that the majority of the information content comes from the measurements and not from the a priori states. It is important to note that a single a priori profile for each species is used for all spectra recorded from 2007 to 2011. This ensures that our observed atmospheric variabilities mainly come from the information content of the measurements.

In the retrieval process, the measured spectrum is weighted by the empirically defined a priori covariance matrix S_a , with diagonal elements reflecting the one-sigma uncertainties used in the OEM. For CO, C₂H₂, CH₃OH, HCOOH, and H₂CO, the off-diagonal elements of S_a correspond to an exponential interlayer correlation with a correlation length of 4 km. For the others species, no interlayer correlation is applied.

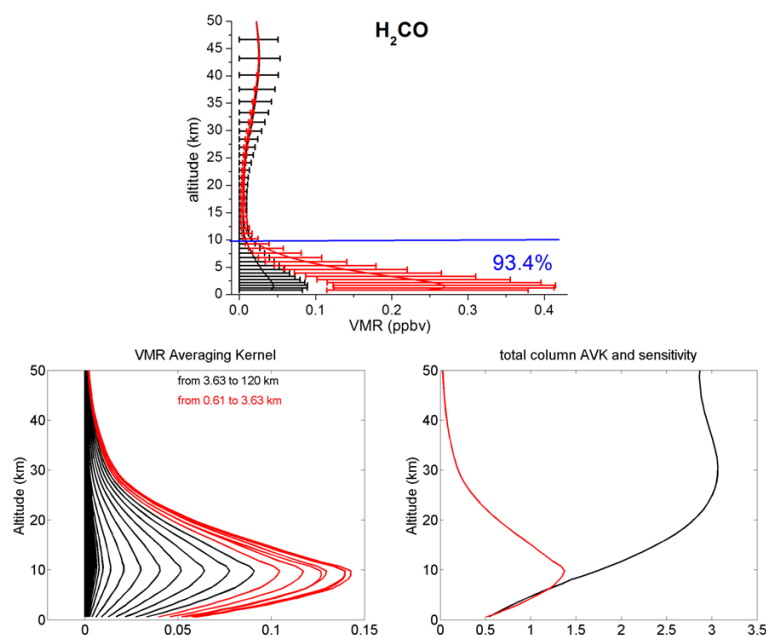


Figure 9. Same as Fig. 3 but for H₂CO. The H₂CO a priori VMR profile is from WACCM v6 and divided by 2.

The relative uncertainties of the a priori VMR profiles (or the standard deviations used in the covariance matrix) are assumed to be 20 % for CO and CH₃OH, 50 % for HCN and C₂H₂, 30 % for C₂H₆ and 100 % for HCOOH and H₂CO, at all altitude layers. These values have been scaled to account for the different thicknesses of the 47 layers in our retrieval scheme. These values, summarized in Table 2, are representative of the tropospheric variabilities derived from the WACCM model, except for CH₃OH and H₂CO. These variabilities are, on average over the troposphere, 17 % for CO, 28 % for HCN, 30 % for C₂H₆ and 66 % for C₂H₂. For CH₃OH, the WACCM model suggests a high tropospheric variability of about 71 %. Since this species has broad absorption features, we prefer to use a lower value of SNR in the retrievals, and then decrease the one-sigma uncertainties to 20 % in the OEM to avoid oscillations in the retrieved profiles. In contrast, the high SNR employed in the HCOOH and H₂CO retrievals, commensurate with the SNR of most analysed spectra, has been compensated for by using large values in the diagonal elements of the a priori covariance matrix. For those two species, the average tropospheric variabilities given by the model are 66 % for HCOOH and 39 % for H₂CO. These variabilities are rather small and not consistent with the idea of an additional large source of HCOOH from snow photochemistry (Dibb and Arseneault, 2002) and the large H₂CO variability of 30 to 700 pptv observed at the Arctic surface (De Serves, 1994).

Finally, the total columns of all the target species are representative of the tropospheric columns. The numbers in blue in Figs. 3 to 9 (upper panels) are the percentages of the tropospheric column contributions (between 0.6 and 10.7 km)

relative to the total column (between 0.6 and 120 km). As can be seen, the tropospheric columns make up more than 90 % of the total columns.

2.5 Averaging kernels

The rows of **A** (Eq. 1) correspond to the averaging kernels for a certain altitude layer and characterize the information content of the retrievals. An ideal observation has an averaging kernel of one in the region of interest and zero outside (Connor et al., 1996). Figures 3 to 9 (lower panels) present the typical VMR averaging kernels, in VMR/VMR (left panels), of the seven retrieved species. The different colours correspond to averaging kernels at altitudes lying in a partial column for which the DOFS is 0.5.

For CO, HCN and C₂H₆, the averaging kernels are more vertically resolved than for the other species, i.e. quasi-independent tropospheric partial columns can be considered between 0.6 and 4 km for CO, between 0.6 and 14 km for HCN, and between 0.6 and 5 km for C₂H₆. Their mean DOFS over 3980, 1815 and 1819 retrievals are 2.5 (± 0.3), 1.6 (± 0.6) and 2.0 (± 0.2), respectively. The numbers in parentheses correspond to the one-sigma standard deviations from the means. For C₂H₂, CH₃OH, HCOOH and H₂CO, the mean DOFS over 1269, 1095, 1973 and 1242 retrievals are 1.1 (± 0.2), 1.2 (± 0.1), 1.1 (± 0.4) and 0.8 (± 0.2), respectively. Total-column averaging kernels, in (molecule cm⁻²)/(molecule cm⁻²), are shown in black lines on the right-hand panels of Figs. 3 to 9 (right-hand lower panels). We have also added the sensitivity profiles of the retrievals to the measurements (Figs. 3 to 9, right-hand lower

Table 3. Error budgets, in percentage, as a function of the different sources of random and systematic uncertainties regarding typical CO, HCN, C₂H₆, C₂H₂, CH₃OH, HCOOH and H₂CO total columns retrieved at PEARL. DOFS and SZA are the acronyms of degrees of freedom for signal and solar zenith angle, respectively.

Error budget (%)	CO	HCN	C ₂ H ₆	C ₂ H ₂	CH ₃ OH	HCOOH	H ₂ CO
N spectra retrieved in time series	3980	1815	1819	1269	1095	1973	1242
DOFS	2.5	1.6	2.0	1.1	1.2	1.1	0.8
Random errors							
Measurement error	0.2	4.3	1.2	7	4.6	16.3	10
Uncertainty regarding temperature	0.7	0.4	0.3	2.9	4.4	2.5	5.5
Uncertainty regarding retrieval parameters	0.3	4.3	2.6	8.2	0	0	1.1
Uncertainty regarding interfering species	0	0.2	0	0.1	0	0.3	24.1
Uncertainty regarding SZA	0.3	0.3	0.3	0.7	0.2	0	0.2
Total random error	0.8	6.1	2.9	11.6	6.3	16.5	26.7
Systematic errors							
Uncertainty regarding line intensity	2.9	4.9	6.4	5.7	10	3.6	2.4
Uncertainty regarding line width	0.4	3.7	2.4	7.7	1.1	0.9	2.1
Total random and systematic error	3.1	8.7	7.4	15.1	11.9	17	26.9
Smoothing error	0.2	5.9	12.2	16.7	3	1.5	5.7
Total error (random + systematic + smoothing)	3.1	10.5	14.3	22.5	12.3	17	27.5

panels, red lines). The sensitivity at a certain altitude is the sum of the elements of the corresponding averaging kernels. It indicates the fraction of the retrievals that comes from the measurements rather than from the a priori information. A sensitivity value of one means that the information content of the retrievals is 100 % from the measurement at this altitude.

All total-column averaging kernels are around one between 0.6 and 10 km, which confirms the good sensitivity of our retrievals in the troposphere. Furthermore, the sensitivity profiles reach one in the troposphere, confirming that the majority of the information content comes from the measurement in this altitude region. For C₂H₆ and C₂H₂, the total-column averaging kernels and sensitivities reach zero at 36 and 22 km, respectively. As a consequence, the retrieved profiles revert to the a priori values above these altitudes (Figs. 3 to 9, upper panels).

2.6 Error budgets

Full error analyses have been performed following the formalism of Rodgers (2000). The error budget is calculated by separating the measurement noise error, the smoothing error (expressing the limited vertical resolution of the retrieval), and the forward model parameter error (including error regarding the temperature profiles, spectroscopic and retrieval parameters, and interfering species uncertainties, and error regarding solar zenith angles). The error analyses have been performed on a representative data set of around 10 spectra per species, selected with different values of solar zenith angle (SZA), SNR, hour and season of measurements. The

averages of all the calculated errors are shown for each target species in Table 3.

The measurement error covariance matrix \mathbf{S}_m is calculated as

$$\mathbf{S}_m = \mathbf{G}_y \mathbf{S}_e \mathbf{G}_y^T, \quad (2)$$

where \mathbf{G}_y is the gain matrix representing the sensitivity of the retrieved parameter to the measurement and \mathbf{S}_e is the measurement covariance matrix as seen in Eq. (1). The diagonal elements of \mathbf{S}_e are the squares of the spectral noise, which is determined by the rms residuals derived from the spectra.

The smoothing error covariance matrix \mathbf{S}_s is calculated as

$$\mathbf{S}_s = (\mathbf{I} - \mathbf{A}) \mathbf{S}_e (\mathbf{I} - \mathbf{A})^T, \quad (3)$$

where \mathbf{I} is the identity matrix, \mathbf{A} is the averaging kernel matrix and \mathbf{S}_e is the climatology matrix representing the natural variability of the target species. The lack of continuous measurements of tropospheric species in the Arctic makes it difficult to build this matrix. Thus, the values derived from WACCM have been used as diagonal elements to express the natural variabilities of each trace gas. For CO, C₂H₂, CH₃OH, HCOOH and H₂CO, the off-diagonal elements of \mathbf{S}_e correspond to an exponential interlayer correlation with a correlation length of 4 km. For the others species, no interlayer correlation is applied, consistent with the retrievals.

Finally the forward parameter error covariance matrix \mathbf{S}_f is calculated as

$$\mathbf{S}_f = (\mathbf{G}_y \mathbf{K}_b) \mathbf{S}_b (\mathbf{G}_y \mathbf{K}_b)^T, \quad (4)$$

where \mathbf{G}_y is the gain matrix and \mathbf{K}_b is the Jacobian matrix obtained by perturbation methods. \mathbf{K}_b represents the sensitivity of the measurements to the model parameter b . \mathbf{S}_b is the covariance error matrix for the parameter b . This parameter b can have systematic (spectroscopic parameters) and random (uncertainties regarding temperature and SZA, for instance) components. To generate the Jacobians, parameters are perturbed by 0.1° for the error regarding SZA, by 2 K for the temperature profiles and by a factor of 1.05 for the line intensity and air-broadened parameters (Batchelor et al., 2009).

In addition to these errors, we have examined the errors for the other retrieved parameters, called interference errors as described in Rodgers and Connor (2003) and explained in detail in Sussmann and Borsdorff (2007) and in Batchelor et al. (2009, Sect. 4). The interference errors combine the errors for the interfering species in the spectral region of interest and the uncertainty due to the retrieval parameters, such as the wavelength shift, the ILS, the background slope and curvature, the zero-level shift and the phase error.

The total random errors are calculated by adding all the uncertainties in quadrature, except the uncertainties regarding line intensity and line width. The predominant contribution to the total random errors is the measurement error for HCN and HCOOH. For CO, the uncertainty regarding temperature is slightly higher than the uncertainty regarding the measurement error, but still remains small. For C₂H₆ and C₂H₂, the measurement error is almost as large as the uncertainties regarding retrieval parameters. This might be an effect of the H₂O continuum, which affects the background slope and curvature of retrievals. For CH₃OH and H₂CO, the temperature uncertainty is high, which is consistent with what has been reported in Vigouroux et al. (2012) for CH₃OH. Concerning H₂CO, the largest random uncertainties come from the uncertainty regarding the interfering species. This might be explained by the fact that H₂CO absorption lines are close to CH₄ lines (in both MWs), which are difficult to fit because of spectroscopic parameter uncertainties (Sussmann et al., 2011). This can also be an effect of the deweighting function used to reduce the SNR of the interfering species in the H₂CO microwindows.

The dominant contribution to the systematic error is the uncertainty regarding the line intensity for all species except C₂H₂, for which the line width uncertainty is larger. For H₂CO, the uncertainties regarding the line width and line intensity are of the same order of magnitude.

As expected, the smoothing error of CO is smaller than for the other species, given the greater DOFS and the tighter averaging kernels.

Unlike the uncertainties regarding the measurement and the spectroscopic parameters, which are considered as truly random and systematic, respectively, some parameters have both components, making the division between those uncertainties difficult. Therefore, the total errors shown in

Table 3 have been determined by adding all these errors in quadrature.

Overall, the total errors of the CO, HCN, C₂H₂, C₂H₆, CH₃OH, HCOOH and H₂CO total columns are 3.1, 10.5, 14.3, 22.5, 12.3, 17.0 and 27.5 %, respectively.

2.7 ACE-FTS measurements

The Atmospheric Chemistry Experiment (ACE) (Bernath et al., 2005) was launched in August 2003 to investigate atmospheric composition mainly in the upper troposphere and the stratosphere. The ACE is equipped with a high-resolution (0.02 cm^{-1}) Fourier transform spectrometer (FTS), operating in the 750 to 4400 cm^{-1} spectral range. It performs solar occultation measurements with limb geometry, with a vertical resolution of about 3–4 km (Boone et al., 2005). VMR profiles of the atmospheric species are retrieved with the version 3.0 algorithm within different altitude ranges for each molecule (<http://www.ace.uwaterloo.ca/molecules.html>; Boone et al., 2013). We chose ACE-FTS measurements for comparison with our new data set because the ACE has good sampling coverage at high latitudes (Bernath, 2006) and measures all seven species of interest in this study.

As shown previously, the ACE-FTS measures VMR profiles of CO (Clerbaux et al., 2008), hydrocarbons, such as HCN, C₂H₆, C₂H₂ (Park et al., 2013) and HCOOH (González Abad et al., 2009) in the upper troposphere and lower stratosphere. In addition to these species, CH₃OH and H₂CO have been measured by the ACE-FTS globally (Dufour et al., 2007, 2009) and in biomass burning plumes over northern high latitudes (Rinsland et al., 2007; Tereszchuk et al., 2011, 2013) and in the Southern Hemisphere (Coheur et al., 2007).

For comparisons with the FTIR data set, all ACE-FTS occultations whose 30 km tangent altitude is within 500 km of PEARL and within 24 h of each FTIR measurement are selected. ACE-FTS data recorded after October 2010 are not used because of an algorithm problem in the version 3.0, which will be fixed in the future version 3.5 (Boone et al., 2013). For the calculations, each ACE-FTS profile was interpolated to the FTIR altitude grid and the FTIR a priori profiles were used to fill the ACE-FTS profiles from the ground to the lowest available ACE-FTS altitudes.

The FTIR and ACE-FTS trace gas profiles are retrieved over different altitude ranges, with different vertical resolutions and sensitivities. To properly account for the different vertical sensitivities of the correlative observations, the ACE-FTS profiles are smoothed by convolution with the FTIR averaging kernel functions, following this equation (Rodgers and Connors, 2003):

$$\mathbf{x}_s = \mathbf{A}(\mathbf{x} - \mathbf{x}_a) + \mathbf{x}_a, \quad (5)$$

where \mathbf{x}_s is the smoothed ACE-FTS profile, \mathbf{A} is the FTIR averaging kernel matrix and \mathbf{x}_a is the FTIR a priori profile.

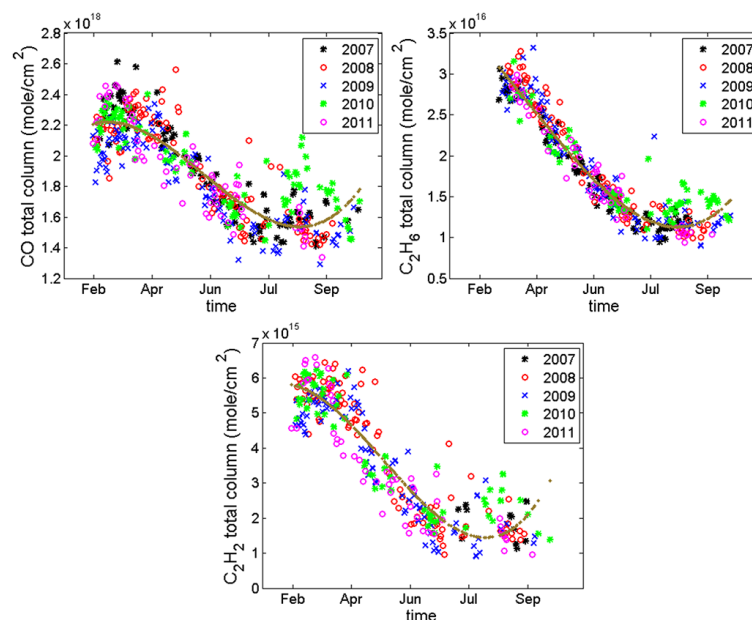


Figure 10. Daily mean total columns (in molecules cm⁻²) of CO, HCN and C₂H₆, plotted in different colours for the different years of measurements. The brown lines show the polynomial fits to the data.

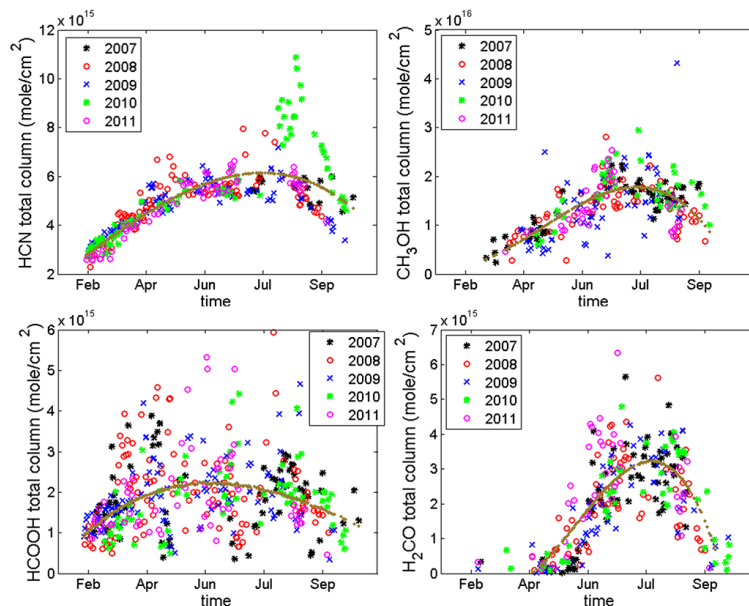


Figure 11. Same as Fig. 10 but for HCN, CH₃OH, HCOOH and H₂CO.

Each partial column is obtained by integration of the trace gas VMR from the lowest to the highest available ACE-FTS level for both the FTIR and ACE-FTS data. Density profiles are obtained by taking the temperature and pressure profiles derived from ACE-FTS measurements.

3 Results and discussion

Seasonal variations of atmospheric concentrations at high latitudes are the largest on earth. Mixing of mid-latitude air into the Arctic occurs typically between mid to late March after the final stratospheric warming (Schoeberl et al., 1992). Since we use a single a priori profile for all the retrievals for a gas, we ensure that the observed variabilities come from the information content of the measurement. The time

series of the daily mean total columns of CO, HCN, C₂H₆, C₂H₂, CH₃OH, HCOOH and H₂CO are plotted in Figs. 10 and 11, using different colours for the different years of measurements from 2007 to 2011. The brown lines represent the polynomial fits to the data. The time series are obtained during the polar-day periods since the FTIR measurements require the sun as a source.

3.1 Seasonal variabilities

3.1.1 Seasonal variabilities of CO, C₂H₆ and C₂H₂

The time series of the CO, C₂H₆ and C₂H₂ total columns show strong seasonal cycles with maxima in winter and minima in summer. These compounds are produced mainly at mid-latitudes. CO is a product of incomplete combustion and atmospheric oxidation of volatile organic compounds (VOCs) and CH₄. The sources of C₂H₆ are natural gas and fossil fuel emissions (Singh and Zimmerman, 1992). C₂H₂ main sources include natural gas, biofuel combustion products and biomass burning emissions (Gupta et al., 1998; Logan et al., 1981; Rudolph, 1995; Xiao et al., 2007; Zhao et al., 2002). CO, C₂H₆ and C₂H₂ are removed by oxidation via OH reaction (Logan et al., 1981), leading to atmospheric lifetimes of approximately fifty-two days (Daniel and Solomon, 1998), eighty days (Xiao et al., 2008) and two weeks in the atmosphere (Xiao et al., 2007), respectively.

The total columns of these three gases are greater in winter because their common sources, which are fossil fuel emissions, are usually enhanced in the dry and cold period (Zhao et al., 2002). In addition, these gases accumulate during this period because their main removal pathway is the reaction with OH, which does not take place in the dark.

The monthly mean total columns for each species are given in Table 5. The percentages of the seasonal variability (or amplitude) are obtained by taking the difference between the maximum and minimum monthly means divided by the annual average for each gas (as described below).

The CO total columns at Eureka have a maximum in March of 2.20×10^{18} molecules cm⁻² (Table 4) and a minimum in September of 1.56×10^{18} molecules cm⁻². The seasonal amplitude of CO total columns is thus estimated to be 34 %. The one-sigma standard deviation from the mean (number in parentheses in Table 4) is slightly higher for the summer months (July and August), reflecting the higher atmospheric variability of CO due to the contribution of boreal forest fire plumes transported from lower latitudes during this period.

The C₂H₆ total columns have a maximum in March of 2.85×10^{16} molecules cm⁻² and a minimum in August of 1.20×10^{16} molecules cm⁻², with a seasonal amplitude of 93 %. The standard deviations around the C₂H₆ monthly means are larger for April and July (Table 4), certainly due to the transport of emissions from extreme fire events during these periods. This is also confirmed by the rather high

standard deviation of the well-known biomass burning tracer HCN, at this time (as described below).

For C₂H₂, the total columns present a maximum in March of 5.50×10^{15} molecules cm⁻² and a minimum in September–October of 1.61×10^{15} molecules cm⁻². Its seasonal cycle of 104 % is larger than for C₂H₆, in agreement with the fact C₂H₂ is more quickly removed by OH reaction (Logan et al., 1981; Singh and Zimmerman, 1992). As seen for C₂H₆, the standard deviations for C₂H₂ are larger for April and July, again due to the greater transport of biomass burning plumes.

Since the lifetimes of these three molecules are rather long (from two weeks to two months, Table 1), the day-to-day variability is attributed to the long-range transport through the Arctic. For instance, the enhanced concentrations in August 2010, represented by the green dots (Fig. 10), have been attributed to an extreme fire event occurring nine days earlier in Russia and transported to Eureka (Viatte et al., 2013). To conclude, we clearly see the combined effect of the chemistry via OH reaction (seasonal variability) and transport (day-to-day variability) in the annual cycles of these three molecules in the high Arctic region.

3.1.2 Seasonal variabilities of HCN, CH₃OH, HCOOH and H₂CO

In contrast to CO, C₂H₆ and C₂H₂, the time series of the HCN, CH₃OH, HCOOH and H₂CO total columns show seasonal cycles with maxima in summer and minima in winter. HCN is a relatively inactive species and is a good tracer of biomass burning emission (Rinsland et al., 2001) with a lifetime of about five months in the troposphere (Li et al., 2003). The reaction with OH and O(¹D) (Cicerone and Zellner, 1983) and ocean uptake (Li et al., 2003) have been shown to be the principal pathways for HCN loss, but its sinks are not well quantified yet (Zeng et al., 2012).

The HCN total columns measured at PEARL have a broad maximum in summer with a sharp increase in August (6.63×10^{15} molecules cm⁻²) due to the plumes from extreme fire events transported to Eureka in summer, and especially in August 2010, when the HCN total columns are enhanced by more than 50 % compared to the four-year average, including all years except 2010 (Viatte et al., 2013). This summer maximum is a result of the combination of emissions by plants, bacteria and fungi due to enhanced vegetative activity in springtime (Cicerone and Zellner, 1983) and biomass burning emissions from boreal forest in summer (Rinsland et al., 2000). The HCN concentrations present a minimum in February of 2.78×10^{15} molecules cm⁻² (Table 4), with a seasonal amplitude of 78 %. In addition, the higher standard deviation for July, August and September, is consistent with severe fire emissions transported from mid-latitudes and the fact that HCN has a long atmospheric lifetime (Table 1).

Table 4. Monthly mean total columns (in molecules cm⁻²) for all trace gases derived in this study from 2007 to 2011. Numbers in parentheses correspond to the one-sigma standard deviation around the monthly mean. The three last rows show the annual means, the one-sigma standard deviation (SD) and the seasonal amplitude in percentage.

Monthly mean total columns	CO × 10 ¹⁸	HCN × 10 ¹⁵	C ₂ H ₆ × 10 ¹⁶	C ₂ H ₂ × 10 ¹⁵	CH ₃ OH × 10 ¹⁶	HCOOH × 10 ¹⁵	H ₂ CO × 10 ¹⁵
February	2.02 (0.11)	2.78 (0.15)		4.57		1.05 (0.25)	
March	2.20 (0.14)	3.37 (0.48)	2.85 (0.14)	5.50 (0.53)	0.42 (0.20)	1.43 (0.64)	0.36 (0.22)
April	2.17 (0.14)	4.58 (0.59)	2.66 (0.28)	5.00 (0.79)	0.74 (0.19)	2.23 (0.93)	0.27 (0.20)
May	1.97 (0.15)	5.39 (0.54)	2.07 (0.21)	3.31 (0.74)	1.08 (0.45)	1.99 (1.05)	0.59 (0.63)
June	1.69 (0.10)	5.58 (0.34)	1.55 (0.15)	2.12 (0.58)	1.57 (0.80)	2.20 (0.86)	2.42 (1.00)
July	1.59 (0.17)	5.76 (0.72)	1.29 (0.24)	1.87 (0.71)	1.82 (0.39)	1.87 (1.05)	3.14 (1.02)
August	1.63 (0.17)	6.63 (1.60)	1.20 (0.17)	1.94 (0.59)	1.53 (0.49)	2.22 (0.88)	2.81 (0.95)
September	1.57 (0.14)	5.28 (1.10)	1.23 (0.18)	1.61 (0.04)	1.36 (0.33)	1.58 (0.72)	1.13 (0.77)
October	1.56 (0.08)	4.69 (0.58)	1.24 (0.03)	1.38		1.14 (0.47)	0.55 (0.38)
Mean	1.89	4.97	1.77	3.95	1.49	1.94	2.30
SD	0.30	1.29	0.65	1.69	0.59	0.90	1.28
Seasonal amplitude (%)	34	78	93	104	94	61	93

Table 5. Comparison of FTIR and ACE-FTS partial columns for all trace gases derived in this study. *N* is the number of coincidences involved in the comparison. The second column gives the mean altitude ranges used for the partial-column calculations, and the third column shows the mean distance of ACE-FTS occultations to PEARL. *R* is the correlation coefficient, and the fifth column gives the values of the slope of the regression plot between the FTIR partial columns and the coincident ACE-FTS measurements along with the 1σ uncertainties of the slopes for each target species.

	<i>N</i>	Mean altitude range for partial columns (km)	Mean distances (km) to PEARL	<i>R</i>	Slope (FTIR vs. ACE-FTS)
CO	106	9.4–48.6	317	0.66	0.97 ± 0.11
HCN	93	7.9–33.2	313	0.96	0.69 ± 0.02
C ₂ H ₆	17	8.0–19.3	436	0.97	0.71 ± 0.04
C ₂ H ₂	93	8.0–17.0	319	0.78	1.21 ± 0.10
CH ₃ OH	6	9.4–17.5	316	0.91	0.74 ± 0.14
HCOOH	103	8.1–18.5	317	0.56	3.35 ± 0.49
H ₂ CO	6	9.1–38.7	317	0.75	0.50 ± 0.22

CH₃OH is the second most abundant volatile organic compound in the atmosphere after CH₄ (Jacob et al., 2005), representing 20 % of the total global VOC emissions (Guenther et al., 2006). Sources include plant growth, ocean and decomposition of plant matter as well as biomass burning emission (Rinsland et al., 2009; Andreae and Merlet, 2001). The principal sink of CH₃OH is chemical loss due to OH reaction (Heikes et al., 2002) leading to the formation of CO and H₂CO (Millet et al., 2006; Rinsland et al., 2009; Stavrakou et al., 2011). The lifetime of CH₃OH in the surface boundary layer is three to six days (Heikes et al., 2002) and between five and ten days on a global scale (Jacob et al., 2005; Stavrakou et al., 2011).

Our CH₃OH total columns have a seasonal amplitude of 94 % with maxima in July of 1.82×10^{16} molecules cm⁻² and minima in March of 0.42×10^{16} molecules cm⁻². This is consistent with ACE-FTS measurements over North America and the role of vegetation growth in this region in driving its seasonal cycle (Dufour et al., 2006). However, biomass burning is a significant source of CH₃OH during summer and the higher standard deviations in June and August confirm the key role of enhanced plant growth and biomass burning at this time.

HCOOH is the second most abundant global organic carboxylic acid in the atmosphere (Zander et al., 2010, and references therein). Direct sources of HCOOH include human activities, biomass burning and plant leaves, and the largest source is the photo-oxidation of NMHCs. HCOOH is removed through oxidation by OH as well as by dry and wet depositions (Stavrakou et al., 2012). However, a recent study suggested a missing source in the HCOOH budget of the northern latitudes and inferred its lifetime to be about three to four days (Paulot et al., 2011).

The HCOOH total columns measured at Eureka show a broad maximum around June of 2.20×10^{15} molecules cm⁻², with two maxima in April and August caused by the activation of biogenic emissions and the presence of intense fire events in those months, respectively. It presents a minimum in February of 1.05×10^{15} molecules cm⁻². This is consistent with the study of Zander et al. (2010), in which the seasonal modulation is in phase with biogenic emissions, which depend on solar isolation, local temperature, atmospheric transport and soil coverage. However, at Eureka, the HCOOH seasonal amplitude of 61 % is smaller than that of the other species, certainly due to the shorter lifetime of this molecule (three

to four days; Table 1) as well as the importance of wet deposition as a sink. Indeed, the smaller standard deviations in February and March might be attributed to the lower winter atmospheric water content, decreasing the effect of wet deposition and resulting in fewer fluctuations in the HCOOH time series. During winter, total columns are affected by the short-range transport with no biogenic emission sources.

Finally, H₂CO is produced by the oxidation of CH₄ and NMHCs, which are emitted into the atmosphere by plants, animals, industrial processes and incomplete combustion of biomass and fossil fuel. Isoprene has also been suggested as an additional significant source of H₂CO (Jones et al., 2009 and references therein). In addition, secondary H₂CO formation in biomass burning plumes has been proposed (Paton-Walsh et al., 2010). It is primarily removed via photodissociation and reaction with OH radicals with a half-life of approximately three hours in daylight (Warneck, 2000) or a lifetime of less than two days (Coheur et al., 2007).

Our H₂CO total columns show a seasonal amplitude of 93 % with summer maxima (in July of 3.14×10^{15} molecules cm⁻²) and late winter minima (in April of 0.27×10^{15} molecules cm⁻²). This is consistent with photochemical control by OH and its formation by CH₄ oxidation in the winter seasons as well as isoprene emissions from plants and forest during the growing season. Most of the seasonal variability corresponds to the biogenic emission and biomass burning events occurring in the boreal summer months.

The seasonal cycles of CH₃OH, HCOOH and H₂CO in the high Arctic are driven by biogenic emissions and short-range transport from lower latitudes, whereas the biomass burning emission and long-range transport affect the seasonal variability of HCN in the Arctic.

Overall, emissions from biomass burning seem to play a significant role in the day-to-day variabilities of the seven tropospheric species observed in the high Arctic.

3.2 Comparisons with the ACE-FTS

The results of the comparisons of the FTIR measurements with those from the ACE-FTS from 2007 to 2010 are given for each molecule in Table 5.

The CO, HCN, C₂H₂ and HCOOH partial columns are compared with all ACE-FTS observations satisfying the coincidence criteria defined in Sect. 2.7; this gives 106, 93, 93 and 103 pairs, respectively. The mean altitude ranges for partial-column calculations are 8.0–48.6 km for CO, 7.9–33.2 km for HCN, 8.0–17.0 km for C₂H₂ and 8.1–18.5 km for HCOOH. For these species, the mean distance of the ACE-FTS occultations (30 km tangent point) to PEARL is between 313 and 319 km. CO, HCN and C₂H₂ partial columns measured by the FTIR are well correlated with the ACE-FTS, with coefficients of correlation (*R*) of 0.66, 0.96 and 0.78. For HCOOH, the agreement is less clear since the coefficient of correlation is 0.56. The FTIR C₂H₆ partial columns,

calculated on average between 8.0 and 19.3 km, are well correlated with the ACE-FTS data. The coefficient of correlation is 0.97 over 17 coincident measurements, with a mean distance to PEARL of 436 km.

The PEARL FTIR and ACE-FTS CO and C₂H₂ partial columns are in good agreement based on the slopes of the regression plots (FTIR vs. ACE-FTS). These values of 0.97 ± 0.11 and 1.21 ± 0.10 suggest no significant bias between the two CO data sets and a positive bias in the FTIR C₂H₂ relative to the ACE-FTS. In contrast, the FTIR HCN and C₂H₆ partial columns are smaller than the ones measured by the ACE-FTS, given the slopes of 0.69 ± 0.02 and 0.71 ± 0.04 , respectively. However, the FTIR HCOOH partial columns are significantly higher than those measured by the ACE-FTS, with a slope of 3.35 ± 0.49 .

For the CH₃OH and H₂CO comparisons, the small number of coincidences (*N* = 6) makes it difficult to draw significant conclusions. The coefficients of correlation between FTIR and ACE-FTS partial columns, calculated on average from 9.4 to 17.5 km for CH₃OH and from 9.1 to 38.7 km, are 0.91 and 0.75, with slopes of 0.74 ± 0.14 and 0.50 ± 0.22 , respectively. It is worth noting that 21 observations were rejected for the H₂CO comparison because they were measured after October 2010. The ACE-FTS algorithm version 3.5 will improve our H₂CO comparisons in the future.

Given the values of the coefficients of correlation and the slopes, the Eureka FTIR measurements of CO, HCN, C₂H₆, C₂H₂ and HCOOH are well correlated with ACE-FTS data, although there are biases between the two data sets, except in the case of CO. For CH₃OH and H₂CO, the small number of coincident profile measurements does not allow us to draw significant conclusions.

3.3 Discussion

Comparisons between our data set and previous measurements reported in the literature lead to a discussion of the atmospheric budget of the different target species observed in the high Arctic.

Our retrieved CO total columns (based on the five-year average) are smaller by a factor of 1.3 compared to CO measured at Ny Ålesund (Norway; 79° N, 12° E) from 1992 to 1995 (Notholt et al., 1997b). This is consistent with the decrease of tropospheric CO of -0.61 ± 0.16 % yr⁻¹ observed at high-latitude sites between 1996 and 2006 (Angelbratt et al., 2011). This trend has been explained by the combination of a 20 % decrease in anthropogenic CO emissions in Europe and North America and 20 % increase in CO anthropogenic emission in east Asia.

Concerning C₂H₆, our total columns are smaller by a factor of 1.1 compared to measurements performed in the Arctic from 1992 to 1995 (Notholt et al., 1997b), suggesting that the Arctic C₂H₆ budget decreased between this period and 2007–2011. This confirms the significant negative trend observed in the Northern Hemisphere at Kiruna (Sweden;

67° N, 20° E) and Harestua (Norway; 60° N, 10° E) from 1996 to 2006 (Angelbratt et al., 2011). Aydin et al. (2011) attributed this trend to the decrease of C₂H₆-based fossil-fuel use in the Northern Hemisphere with the possibility that an increase in chlorine atoms plays a role in the C₂H₆ decline. Recent studies also evaluated a negative trend in the Southern Hemisphere at Lauder (New Zealand; 45° S, 170° E) and Arrival Height (Antarctica; 78° S, 167° E) from 1997 to 2009 as well as at Wollongong (Australia; 34° S, 150° E) (Zeng et al., 2012).

For C₂H₂, our total-column values and seasonal variability are in agreement with values reported at Reunion Island (France; 21° S, 55° E) from 2004 to 2011 (Vigouroux et al., 2012) and at Jungfraujoch station (Switzerland; 46° N, 8° E) from 1995 to 2008 (Mahieu et al., 2008) as well as at Ny Ålesund from 1992 to 1999 (Albrecht et al., 2002). The similarity between high-latitude and mid-latitude C₂H₂ concentrations has already been reported (Albrecht et al., 2002) and highlights the importance of transport for the C₂H₂ budget in the Arctic. However, the primary source of C₂H₂ is transportation at mid-latitudes (Xiao et al., 2007). So the reason for the fact that our C₂H₂ total columns are comparable to those measured in the Arctic between 1992 and 1999 (i.e. no decrease is seen from previous years compared to the observed decline of CO or C₂H₆) is unclear. One hypothesis might be that C₂H₂ emissions from cars have not changed compared to the technological advances in the catalytic converters employed to reduce CO and C₂H₆ emissions.

Our HCN total columns are of the same order of magnitude, in term of absolute values and variabilities, as those reported by Notholt et al. (1997b) in the Arctic from 1992 to 1995. They also agree well with HCN columns observed at mid-latitude regions, as in northern Japan at 44° N in 1995 (Zhao et al., 2000) as well as at Jungfraujoch from 2001 to 2009 (Li et al., 2009). In addition, our extreme values, exceeding 10×10^{15} molecules cm⁻² in summer 2010, are comparable to values found in the tropics at Reunion Island during the biomass burning seasons from 2004 to 2011 (Vigouroux et al., 2012). This confirms the key role of the transport from mid-latitudes in the HCN budget at high-latitudes. However, a negative trend has been highlighted in the Southern Hemisphere for the tropospheric HCN columns observed at Lauder (New Zealand; 45° S, 170° E) from 1997 to 2009 (Zeng et al., 2012), which is not seen in our data. This may be due to the fact that during the five years of HCN measurements at Eureka, several extreme biomass burning events were detected, especially a persistent and intense one in August 2010 (Viatte et al., 2013).

Concerning CH₃OH, our total columns are of the same order of magnitude as those of Vigouroux et al. (2012) and Bader et al. (2013) obtained at Reunion Island and Jungfraujoch station, respectively. In the latter study, extreme enhancements were shown to reach 2.5×10^{16} molecules cm⁻², in agreement with our high total columns in the June months. Furthermore, the difference

between the largest and the smallest individual columns at Jungfraujoch station exceeds a factor of 14, which is in excellent agreement with the observed variability at Eureka. Finally, our monthly mean total columns show a factor of four in the seasonal amplitude, comparable to a factor three of variation found for free tropospheric CH₃OH columns at Kitt Peak (United States; 32° N, 111° W) over 22 years of observations (Rinsland et al., 2009).

Our HCOOH retrieved columns are in agreement in terms of mean and extreme values as well as seasonal amplitude, compared to those measured at Jungfraujoch (Zander et al., 2010). They reported a mean value of $1.70 \pm 0.50 \times 10^{15}$ molecules cm⁻² for June–July–August from 1985 to 2007, which is comparable to our average of $2.10 \pm 0.20 \times 10^{15}$ molecule cm⁻² for the same summer months from 2007 to 2011. Also, our outliers are enhanced by a factor of four relative to the monthly means, which is in agreement with the large variability of HCOOH columns measured at Jungfraujoch. However, our seasonal variability is less clear than at mid-latitudes, certainly due to the contribution of the short-range transport and the importance of wet deposition as a sink of HCOOH. Finally, HCOOH total columns have been recently obtained with ground-based FTIR measurements at Thule in the Arctic (Greenland; 76° N, 69° W) from 2004 to 2009 (Paulot et al., 2011, their Fig. 3). Excellent agreement, in terms of seasonal variability and extreme values, is seen with this data set, with higher values in 2008 (red circles in our Fig. 11) due to exceptional biomass burning in Asian boreal forests (Giglio et al., 2010).

Finally, our H₂CO total columns, which vary from 1.90×10^{13} to 6.3×10^{15} molecules cm⁻² with an annual average of 2.3×10^{15} molecules cm⁻² (between February and October), are lower than those found in the literature, especially those for the spring and autumn. For instance, Notholt et al. (1997b) reported Arctic total columns varying from around 2 to 8×10^{15} molecules cm⁻² between 1992 and 1998 at Ny Ålesund. Part of this difference might be attributed to the use of updated line strengths in HITRAN 2008. Indeed, the new spectroscopic intensities have been increased by around 30 % in the spectral region employed here (Perrin et al., 2009), leading to a significant decrease of the retrieved total columns. In addition, Jones et al. (2009) showed columns from around 2.5 to 8×10^{15} molecules cm⁻² between 1992 and 2004 at Lauder (New Zealand; 45° S, 170° E), and Vigouroux et al. (2009) measured columns from 1.6 to 7×10^{15} molecules cm⁻² at Reunion Island (France; 21° S, 55° E) between 2004 and 2011. Our low H₂CO total columns measured in late winter might also reflect the large atmospheric variability of H₂CO, given its small lifetime, with no local sources in winter at Eureka. However, our data show a strong seasonal cycle consistent with the FTIR measurements at Ny Ålesund (Albrecht et al., 2002) and in situ measurements at Alert (Canada; 82° N, 63° W), which range from 30 to 700 pptv (De Serves, 1994).

4 Summary and conclusions

The ground-based FTIR technique is a powerful tool for deriving long-term measurements of various atmospheric species having both natural and anthropogenic sources. Monitoring tropospheric molecules with different atmospheric lifetimes and origins provides useful information about chemical and physical processes in the Arctic, such as transport (Shindell et al., 2008) and the degradation mechanisms of non-methane hydrocarbons (Stavrakou et al., 2009), which need to be better understood in model simulations (Millet et al., 2008; Parker et al., 2011; Paulot et al., 2011). Our ground-based FTIR measurements at PEARL constitute a new Arctic data set of seven tropospheric species, CO, HCN, C₂H₆, C₂H₂, CH₃OH, HCOOH and H₂CO, observed from 2007 to 2011. The total columns of CH₃OH are the first to be reported from ground-based FTIR measurements in the high Arctic.

The different lifetimes of these tropospheric molecules, from less than two days to six months, play a role in their observed seasonal variabilities at PEARL. The seasonal variability provides additional evidence of the interplay between chemistry and transport, which will help to constrain global atmospheric chemical transport models. The time series of the CO, C₂H₆ and C₂H₂ total columns show strong seasonal amplitudes of 34, 93 and 104 %, respectively, with maxima in winter and minima in summer. These seasonal cycles highlight the combined effect of the chemistry via OH reaction (seasonal variability) and long-range transport (day-to-day variability) in the Arctic budget of CO, C₂H₆ and C₂H₂. In contrast to these molecules, the time series of the HCN, CH₃OH, HCOOH and H₂CO total columns show seasonal amplitudes of 78, 94, 61 and 93 %, respectively, with maxima in summer and minima in winter. These seasonal cycles are driven by biogenic emissions and short-range transport for CH₃OH, HCOOH and H₂CO, and biomass burning emissions and long-range transport for HCN. Overall, emissions from biomass burning seem to play a significant role in the day-to-day variability of the seven tropospheric species observed in the high Arctic. This data set highlights the importance of the transport of pollutants from lower latitudes and can be used to assess the influx of pollution into the sensitive area of the Arctic.

In order to assess our new data set, the ACE-FTS satellite instrument was selected since it has good sampling in the Arctic and measures all seven species studied here. Given the values of the coefficients of correlation and the slopes, ranging from 0.56 to 0.97 and from 0.71 to 3.35, respectively, the FTIR measurements at Eureka of CO, HCN, C₂H₆, C₂H₂ and HCOOH are generally well correlated with the ACE-FTS data, although there are biases between the two data sets. For CH₃OH and H₂CO, the small number of coincidences (six pairs) does not allow us to draw meaningful conclusions.

Finally, our new data set has been compared to previous published measurements. Our measurements are consistent with the negative trends of CO and C₂H₆ observed over the Northern Hemisphere, which have been attributed to decreasing fossil fuel emissions. The similarity of the HCN and C₂H₂ concentrations between mid- and high latitudes highlights the importance of transport for the atmospheric budget of these molecules in the Arctic. Concentrations and seasonal cycles of CH₃OH and HCOOH at PEARL are comparable with previous measurements performed at remote sites. Excellent agreement is found between our HCOOH total columns and measurements from Thule (Paulot et al., 2011). However, the atmospheric concentrations of H₂CO at PEARL in the early spring are smaller than those reported in the literature. This might reflect the large atmospheric variability of H₂CO, given its short lifetime with no local sources in winter at Eureka, and/or the effect of the updated spectroscopic parameters used in our retrievals.

To conclude, our measurements of tropospheric species at Eureka constitute a new data set which can be used as a constraint to improve the model simulations of chemical and dynamical processes in the high Arctic. Comparisons of the FTIR measurements with two chemical-transport models are in progress. In addition, since all seven molecules are biomass burning products, they can be used to identify fire events in order to study the chemical composition of the plumes above PEARL and to derive emission ratios, which are key parameters needed to simulate fire emissions in atmospheric models.

Acknowledgements. The PEARL Bruker 125HR measurements at Eureka were carried out by the Canadian Network for the Detection of Atmospheric Change (CANDAC), which was supported by the Atlantic Innovation Fund/Nova Scotia Research and Innovation Trust, the Canada Foundation for Innovation, the Canadian Foundation for Climate and Atmospheric Sciences, the Canadian Space Agency (CSA), Environment Canada, Government of Canada International Polar Year funding, the Natural Sciences and Engineering Research Council of Canada, the Ontario Innovation Trust, the Ontario Research Fund, and the Polar Continental Shelf Program. The authors wish to thank the staff at Environment Canada's Eureka Weather Station and CANDAC for logistical and on-site support. Thanks to Rodica Lindenmaier, Rebecca Batchelor and PEARL Site Manager Pierre Fogal as well as CANDAC/PEARL operators Ashley Harrett, Alexei Khmel, Paul Loewen, Keith MacQuarrie, Oleg Mikhailov and Matt Okraszewski for their invaluable assistance in maintaining and operating the Bruker 125HR. The Atmospheric Chemistry Experiment is a Canadian-led mission mainly supported by the CSA.

Edited by: M. Van Roozendael

References

- Albrecht, T., Notholt, J., Wolke, R., Solberg, S., Dye, C., and Malberg, H.: Variations of CH₂O and C₂H₂ determined from ground-based FTIR measurements and comparison with model results, *Adv. Space Res.*, 29, 1713–1718, doi:10.1016/S0273-1177(02)00120-5, 2002.
- Andreae, M. O. and Merlet, P.: Emission of trace gases and aerosols from biomass burning, *Global Biogeochem. Cy.*, 15, 955–966, doi:10.1029/2000GB001382, 2001.
- Angelbratt, J., Mellqvist, J., Blumenstock, T., Borsdorff, T., Brohede, S., Duchatelet, P., Forster, F., Hase, F., Mahieu, E., Murtagh, D., Petersen, A. K., Schneider, M., Sussmann, R., and Urban, J.: A new method to detect long term trends of methane (CH₄) and nitrous oxide (N₂O) total columns measured within the NDACC ground-based high resolution solar FTIR network, *Atmos. Chem. Phys.*, 11, 6167–6183, doi:10.5194/acp-11-6167-2011, 2011.
- Aydin, M., Verhulst, K. R., Saltzman, E. S., Battle, M. O., Montzka, S. A., Blake, D. R., Tang, Q., and Prather, M. J.: Recent decreases in fossil-fuel emissions of ethane and methane derived from firn air, *Nature*, 476, 198–201, doi:10.1038/nature10352, 2011.
- Baboukas, E. D., Kanakidou, M., and Mihalopoulos, N.: Carboxylic acids in gas and particulate phase above the Atlantic Ocean, *J. Geophys. Res.*, 105, 14459–14471, doi:10.1029/1999JD900977, 2000.
- Bader, W., Mahieu, E., Bovy, B., Lejeune, B., Demoulin, P., Servais, C., and Harrison, J. J.: Evolution of methanol (CH₃OH) above the Jungfraujoch station (46.5° N): variability, seasonal modulation and long-term trend, *Geophys. Res. Abstr.*, 15, EGU2013-1471, 2013.
- Barret, B., De Mazière, M., and Mahieu, E.: Ground-based FTIR measurements of CO from the Jungfraujoch: characterisation and comparison with in situ surface and MOPITT data, *Atmos. Chem. Phys.*, 3, 2217–2223, doi:10.5194/acp-3-2217-2003, 2003.
- Batchelor, R. L., Strong, K., Lindenmaier, R. L., Mittermeier, R., Fast, H., Drummond, J. R., and Fogal, P. F.: A new Bruker IFS 125HR FTIR spectrometer for the Polar Environment Atmospheric Research Laboratory at Nunavut, Canada: Measurements and comparison with the existing Bomem DA8 spectrometer, *J. Atmos. Ocean. Tech.*, 26, 1328–1340, doi:10.1175/2009JTECHA1215.1, 2009.
- Bernath, P. F.: Atmospheric Chemistry Experiment (ACE): Analytical Chemistry from Orbit, *Trends Anal. Chem.*, 25, 647–654, doi:10.1016/j.trac.2006.05.001, 2006.
- Bernath, P. F., McElroy, C. T., Abrams, M. C., Boone, C. D., Butler, M., Camy-Peyret, C., Carleer, M., Clerbaux, C., Coheur, P.-F., Colin, R., DeCola, P., DeMazière, M., Drummond, J. R., Dufour, D., Evans, W. F. J., Fast, H., Fussen, D., Gilbert, K., Jennings, D. E., Llewellyn, E. J., Lowe, R. P., Mahieu, E., McConnell, J. C., McHugh, M., McLeod, S. D., Michaud, R., Midwinter, C., Nassar, R., Nichitiu, F., Nowlan, C., Rinsland, C. P., Rochon, Y. J., Rowlands, N., Semeniuk, K., Simon, P., Skelton, R., Sloan, J. J., Soucy, M.-A., Strong, K., Tremblay, P., Turnbull, D., Walker, K. A., Walkty, I., Wardle, D. A., Wehrle, V., Zander, R., and Zou, J.: Atmospheric Chemistry Experiment (ACE): mission overview, *Geophys. Res. Lett.*, 32, L15S01, doi:10.1029/2005GL022386, 2005.
- Boone, C. D., Nassar, R., Walker, K. A., Rochon, Y., McLeod, S. D., Rinsland, C. P., and Bernath, P. F.: Retrievals for the Atmospheric Chemistry Experiment Fourier Transform Spectrometer, *Appl. Optics*, 44, 7218–7231, 2005.
- Boone, C. D., Walker, K. A., and Bernath, P. F.: Version 3 retrievals for the Atmospheric Chemistry Experiment Fourier Transform Spectrometer (ACE-FTS), in: Chapter 6 in the Atmospheric Chemistry Experiment ACE at 10: A solar Occultation Anthology, edited by: Bernath, P. F., A. Deepak Publishing, Hampton, VA, in press, 103–127, 2013.
- Cicerone, R. J. and Zellner, R.: The atmospheric chemistry of hydrogen cyanide (HCN), *J. Geophys. Res.*, 88, 10689–10696, doi:10.1029/JC088iC15p10689, 1983.
- Clerbaux, C., George, M., Turquety, S., Walker, K. A., Barret, B., Bernath, P., Boone, C., Borsdorff, T., Cammas, J. P., Catoire, V., Coffey, M., Coheur, P.-F., Deeter, M., De Mazière, M., Drummond, J., Duchatelet, P., Dupuy, E., de Zafra, R., Eddounia, F., Edwards, D. P., Emmons, L., Funke, B., Gille, J., Griffith, D. W. T., Hannigan, J., Hase, F., Höpfner, M., Jones, N., Kagawa, A., Kasai, Y., Kramer, I., Le Flochmoën, E., Livesey, N. J., López-Puertas, M., Luo, M., Mahieu, E., Murtagh, D., Nédélec, P., Pazmino, A., Pumphrey, H., Ricaud, P., Rinsland, C. P., Robert, C., Schneider, M., Senten, C., Stiller, G., Strandberg, A., Strong, K., Sussmann, R., Thouret, V., Urban, J., and Wiacek, A.: CO measurements from the ACE-FTS satellite instrument: data analysis and validation using ground-based, airborne and spaceborne observations, *Atmos. Chem. Phys.*, 8, 2569–2594, doi:10.5194/acp-8-2569-2008, 2008.
- Coheur, P.-F., Herbin, H., Clerbaux, C., Hurtmans, D., Wespes, C., Carleer, M., Turquety, S., Rinsland, C. P., Remedios, J., Hauglustaine, D., Boone, C. D., and Bernath, P. F.: ACE-FTS observation of a young biomass burning plume: first reported measurements of C₂H₄, C₃H₆O, H₂CO and PAN by infrared occultation from space, *Atmos. Chem. Phys.*, 7, 5437–5446, doi:10.5194/acp-7-5437-2007, 2007.
- Connor, B. J., Jones, N. B., Wood, S. W., Keys, J. G., Rinsland, C. P., and Murcray, F. J.: Retrieval of HCl and HNO profiles from ground-based FTIR data using SFIT2, in: Proceedings of 18th Quadrennial Ozone Symposium, edited by: Bojkov, R. and Visconti, G., Parco Sci. e Technol. D'Abruzzo, L'Aquila, Italy, 485–488, 1996.
- Daniel, J. S. and Solomon, S.: On the climate forcing of carbon monoxide, *J. Geophys. Res.*, 103, 13249–13260, doi:10.1029/98JD00822, 1998.
- De Serves, C.: Gas phase formaldehyde and peroxide measurements in the Arctic atmosphere, *J. Geophys. Res.*, 99, 25391–25398, doi:10.1029/94JD00547, 1994.
- Dibb, J. E. and Arsenault, M.: Shouldn't snowpacks be sources of monocarboxylic acids?, *Atmos. Environ.*, 36, 2513–2522, doi:10.1016/S1352-2310(02)00131-0, 2002.
- Dufour, G., Boone, C. D., Rinsland, C. P., and Bernath, P. F.: First space-borne measurements of methanol inside aged southern tropical to mid-latitude biomass burning plumes using the ACE-FTS instrument, *Atmos. Chem. Phys.*, 6, 3463–3470, doi:10.5194/acp-6-3463-2006, 2006.

- Dufour, G., Szopa, S., Hauglustaine, D. A., Boone, C. D., Rinsland, C. P., and Bernath, P. F.: The influence of biogenic emissions on upper-tropospheric methanol as revealed from space, *Atmos. Chem. Phys.*, 7, 6119–6129, doi:10.5194/acp-7-6119-2007, 2007.
- Dufour, G., Szopa, S., Barkley, M. P., Boone, C. D., Perrin, A., Palmer, P. I., and Bernath, P. F.: Global upper-tropospheric formaldehyde: seasonal cycles observed by the ACE-FTS satellite instrument, *Atmos. Chem. Phys.*, 9, 3893–3910, doi:10.5194/acp-9-3893-2009, 2009.
- Eckhardt, S., Stohl, A., Beirle, S., Spichtinger, N., James, P., Forster, C., Junker, C., Wagner, T., Platt, U., and Jennings, S. G.: The North Atlantic Oscillation controls air pollution transport to the Arctic, *Atmos. Chem. Phys.*, 3, 1769–1778, doi:10.5194/acp-3-1769-2003, 2003.
- Fisher, J. A., Jacob, D. J., Purdy, M. T., Kopacz, M., Le Sager, P., Carouge, C., Holmes, C. D., Yantosca, R. M., Batchelor, R. L., Strong, K., Diskin, G. S., Fuelberg, H. E., Holloway, J. S., Hyer, E. J., McMillan, W. W., Warner, J., Streets, D. G., Zhang, Q., Wang, Y., and Wu, S.: Source attribution and interannual variability of Arctic pollution in spring constrained by aircraft (ARCTAS, ARCPAC) and satellite (AIRS) observations of carbon monoxide, *Atmos. Chem. Phys.*, 10, 977–996, doi:10.5194/acp-10-977-2010, 2010.
- Fogal, P. F., LeBlanc, L. M., and Drummond, J. R.: The Polar Environment Atmospheric Research Laboratory (PEARL): Sounding the Atmosphere at 80° North, Arctic, 66, 377–386, 2013.
- Giglio, L., Randerson, J. T., van der Werf, G. R., Kasibhatla, P. S., Collatz, G. J., Morton, D. C., and DeFries, R. S.: Assessing variability and long-term trends in burned area by merging multiple satellite fire products, *Biogeosciences*, 7, 1171–1186, doi:10.5194/bg-7-1171-2010, 2010.
- Glatthor, N., von Clarmann, T., Stiller, G. P., Funke, B., Koukoulis, M. E., Fischer, H., Grabowski, U., Höpfner, M., Kellmann, S., and Linden, A.: Large-scale upper tropospheric pollution observed by MIPAS HCN and C₂H₆ global distributions, *Atmos. Chem. Phys.*, 9, 9619–9634, doi:10.5194/acp-9-9619-2009, 2009.
- González Abad, G., Bernath, P. F., Boone, C. D., McLeod, S. D., Manney, G. L., and Toon, G. C.: Global distribution of upper tropospheric formic acid from the ACE-FTS, *Atmos. Chem. Phys.*, 9, 8039–8047, doi:10.5194/acp-9-8039-2009, 2009.
- Goode, J., Yokelson, R., Ward, D., Susott, R., Babbitt, R., Davies, M., and Hao, W.: Measurements of excess O₃, CO₂, CO, CH₄, C₂H₄, C₂H₂, HCN, NO, NH₃, HCOOH, CH₃COOH, HCHO, and CH₃OH in 1997 Alaskan biomass burning plumes by air borne Fourier transform infrared spectroscopy (AFTIR), *J. Geophys. Res.*, 105, 22147–22166, doi:10.1029/2000JD900287, 2000.
- Grutter, M., Glatthor, N., Stiller, G., Fischer, H., Grabowski, U., Höpfner, M., Kellmann, S., Linden, A., and von Clarmann, T.: Global distribution and variability of formic acid as observed by MIPAS-ENVISAT, *J. Geophys. Res.*, 115, D10303, doi:10.1029/2009JD012980, 2010.
- Guenther, A., Karl, T., Harley, P., Wiedinmyer, C., Palmer, P. I., and Geron, C.: Estimates of global terrestrial isoprene emissions using MEGAN (Model of Emissions of Gases and Aerosols from Nature), *Atmos. Chem. Phys.*, 6, 3181–3210, doi:10.5194/acp-6-3181-2006, 2006.
- Gupta, M. L., Cicerone, R. J., Blake, D. R., Rowland, F. S., and Isaksen, I. S. A.: Global atmospheric distributions and source strengths of light hydrocarbons and tetrachloroethene, *J. Geophys. Res.*, 103, 28219–28235, doi:10.1029/98JD02645, 1998.
- Hak, C., Pundt, I., Trick, S., Kern, C., Platt, U., Dommen, J., Ordóñez, C., Prévôt, A. S. H., Junkermann, W., Astorga-Lloréns, C., Larsen, B. R., Mellqvist, J., Strandberg, A., Yu, Y., Galle, B., Kleffmann, J., Lörzer, J. C., Braathen, G. O., and Volkamer, R.: Intercomparison of four different in-situ techniques for ambient formaldehyde measurements in urban air, *Atmos. Chem. Phys.*, 5, 2881–2900, doi:10.5194/acp-5-2881-2005, 2005.
- Hase, F., Blumenstock, T., and Paton-Walsh, C.: Analysis of the instrumental line shape of high-resolution Fourier transform IR spectrometers with gas cell measurements and new retrieval software, *Appl. Optics*, 38, 3417–3422, doi:10.1364/AO.38.003417, 1999.
- Heikes, B., Chang, W., Pilson, M., Swift, E., Singh, H., Guenther, A. B., Jacob, D., Field, B., Fall, R., Riemer, D., and Brand, L.: Atmospheric methanol budget and ocean implication, *Global Biogeochem. Cy.*, 16, 1133, doi:10.1029/2002GB001895, 2002.
- IPCC – Intergovernmental Panel on Climate Change: Climate Change 2007: The physical science basis, in: chapter 7, Coupling Between Changes in the Climate System and Biogeochemistry, edited by: Solomon, S., Quin, D., Manning, M., Chen, Z., Marquis, M., Averyt, K. B., Tignor, M., and Miller, H. L., Cambridge University Press, Cambridge, UK, 500–657, 2007.
- Jacob, D. J., Field, B. D., Li, Q., Blake, D. R., de Gouw, J., Warneke, C., Hansel, A., Wisthaler, A., Singh, H. B., and Guenther, A.: Global budget of methanol: Constraints from atmospheric observations, *J. Geophys. Res.*, 110, D08303, doi:10.1029/2004JD005172, 2005.
- Jacob, D. J., Crawford, J. H., Maring, H., Clarke, A. D., Dibb, J. E., Emmons, L. K., Ferrare, R. A., Hostetler, C. A., Russell, P. B., Singh, H. B., Thompson, A. M., Shaw, G. E., McCauley, E., Pederson, J. R., and Fisher, J. A.: The Arctic Research of the Composition of the Troposphere from Aircraft and Satellites (ARCTAS) mission: design, execution, and first results, *Atmos. Chem. Phys.*, 10, 5191–5212, doi:10.5194/acp-10-5191-2010, 2010.
- Jones, N. B., Riedel, K., Allan, W., Wood, S., Palmer, P. I., Chance, K., and Notholt, J.: Long-term tropospheric formaldehyde concentrations deduced from ground-based fourier transform solar infrared measurements, *Atmos. Chem. Phys.*, 9, 7131–7142, doi:10.5194/acp-9-7131-2009, 2009.
- Klonecki, A., Hess, P., Emmons, L., Smith, L., Orlando, J., and Blake, D.: Seasonal changes in the transport of pollutants into the Arctic troposphere-model study, *J. Geophys. Res.*, 108, 8367, doi:10.1029/2002JD002199, 2003.
- Koch, D. and Hansen, J.: Distant origins of Arctic black carbon: A Goddard Institute for Space Studies ModelE experiment, *J. Geophys. Res.*, 110, D04204, doi:10.1029/2004JD005296, 2005.
- Le Breton, M., Bacak, A., Muller, J. B. A., O'Shea, S. J., Xiao, P., Ashfold, M. N. R., Cooke, M. C., Batt, R., Shallcross, D. E., Oram, D. E., Forster, G., Bauguutte, S. J.-B., Palmer, P. I., Parrington, M., Lewis, A. C., Lee, J. D., and Percival, C. J.: Airborne hydrogen cyanide measurements using a chemical ionisation mass spectrometer for the plume identification of biomass burning forest fires, *Atmos. Chem. Phys.*, 13, 9217–9232, doi:10.5194/acp-13-9217-2013, 2013.

- Lesins, G., Duck, T. J., and Drummond, J. R.: Climate trends at Eureka in the Canadian high Arctic, *Atmos. Ocean*, 48, 59–80, doi:10.3137/AO1103.2010, 2010.
- Li, Q., Jacob, D. J., Yantosca, R. M., Heald, C. L., Singh, H. B., Koike, M., Zhao, Y., Sachse, G. W., and Streets, D. G.: A global three-dimensional model analysis of the atmospheric budgets of HCN and CH₃CN: Constraints from aircraft and ground measurements, *J. Geophys. Res.*, 108, 8827, doi:10.1029/2002JD003075, 2003.
- Li, Q., Palmer, P. I., Pumphrey, H. C., Bernath, P., and Mahieu, E.: What drives the observed variability of HCN in the troposphere and lower stratosphere?, *Atmos. Chem. Phys.*, 9, 8531–8543, doi:10.5194/acp-9-8531-2009, 2009.
- Lindenmaier, R.: Studies of Arctic middle atmosphere chemistry using infrared absorption spectroscopy, Ph.D. Thesis, University of Toronto, Toronto, Canada, 2012.
- Logan, J. A., Prather, M. J., Wofsy, S. C., and McElroy, M. B.: Tropospheric chemistry: a global perspective, *J. Geophys. Res.*, 86, 7210–7254, doi:10.1029/JC086iC08p07210, 1981.
- Mahieu, E., Zander, R., Delbouille, L., Demoulin, P., Roland, G., and Servais, C.: Observed trends in total vertical column abundances of atmospheric gases from IR solar spectra recorded at the Jungfraujoch, *J. Atmos. Chem.*, 28, 227–243, doi:10.1023/A:1005854926740, 1997.
- Mahieu, E., Duchatelet, P., Bernath, P. F., Boone, C. D., De Maziere, M., Demoulin, P., Rinsland, C. P., Servais, C., and Walker, K. A.: Retrievals of C₂H₂ from high-resolution FTIR solar spectra recorded at the Jungfraujoch station (46.5° N) and comparison with ACE-FTS observations, *Geophys. Res. Abstr.*, 10, EGU2008-A-00000, 2008.
- Meier, A., Toon, G. C., Rinsland, C. P., Goldman, A., and Hase, F.: Spectroscopic atlas of atmospheric microwindows in the middle infrared, 2nd revised Edn., IRF Technical Report 048, IRF – Institutet för Rymdfysik, Kiruna, Sweden, 2004.
- Millet, D. B., Jacob, D. J., Turquety, S., Hudman, R. C., Wu, S., Fried, A., Walega, J., Heikes, B. G., Blake, D. R., Singh, H. B., Anderson, B. E., and Clarke, A. D.: Formaldehyde distribution over North America: Implications for satellite retrievals of formaldehyde columns and isoprene emission, *J. Geophys. Res.*, 111, D24S02, doi:10.1029/2005JD006853, 2006.
- Millet, D. B., Jacob, D. J., Custer, T. G., de Gouw, J. A., Goldstein, A. H., Karl, T., Singh, H. B., Sive, B. C., Talbot, R. W., Warneke, C., and Williams, J.: New constraints on terrestrial and oceanic sources of atmospheric methanol, *Atmos. Chem. Phys.*, 8, 6887–6905, doi:10.5194/acp-8-6887-2008, 2008.
- Notholt, J., Toon, G. C., Lehmann, R., Sen, B., and Blavier, J.-F.: Comparison of Arctic and Antarctic trace gas column abundances from ground-based Fourier transform infrared spectrometry, *J. Geophys. Res.*, 102, 12863–12869, doi:10.1029/97JD00358, 1997a.
- Notholt, J., Toon, G., Stordal, F., Solberg, S., Schmidbauer, N., Becker, E., Meier, A., and Sen, B.: Seasonal variations of atmospheric trace gases in the high Arctic at 79° N, *J. Geophys. Res.*, 102, 12855–12861, doi:10.1029/97JD00337, 1997b.
- Notholt, J., Toon, G. C., Rinsland, C. P., Pougetchev, N. S., Jones, N. B., Connor, B. J., Weller, R., Gautrois, M., and Schrems, O.: Latitudinal variations of trace gas concentrations measured by solar absorption spectroscopy during a ship cruise, *J. Geophys. Res.*, 105, 1337–1349, doi:10.1029/1999JD900940, 2000.
- Park, M., Randel, W. J., Kinnison, D. E., Emmons, L. K., Bernath, P. F., Walker, K. A., Boone, C. D. D., and Livesey, N. J.: Hydrocarbons in the upper troposphere and lower stratosphere observed from ACE-FTS and comparisons with WACCM, *J. Geophys. Res. Atmos.*, 118, 1–17, doi:10.1029/2012JD018327, 2013.
- Parker, R. J., Remedios, J. J., Moore, D. P., and Kanawade, V. P.: Acetylene C₂H₂ retrievals from MIPAS data and regions of enhanced upper tropospheric concentrations in August 2003, *Atmos. Chem. Phys.*, 11, 10243–10257, doi:10.5194/acp-11-10243-2011, 2011.
- Paton-Walsh, C.: Measurements and Modelling of Emissions from Biomass Burning in Australia, Ph.D. Thesis, University of Wollongong, Wollongong, p. 45, 2009.
- Paton-Walsh, C., Jones, N. B., Wilson, S. R., Harverd, V., Meier, A., Griffith, D. W. T., and Rinsland, C. P.: Measurements of trace gas emissions from Australian forest fires and correlations with coincident measurements of aerosol optical depth, *J. Geophys. Res.*, 110, D24305, doi:10.1029/2005JD006202, 2005.
- Paton-Walsh, C., Wilson, S. R., Jones, N. B., and Griffith, D. W. T.: Measurement of methanol emissions from Australian wildfires by ground-based solar Fourier transform spectroscopy, *Geophys. Res. Lett.*, 35, L08810, doi:10.1029/2007GL032951, 2008.
- Paton-Walsh, C., Deutscher, N. M., Griffith, D. W. T., Forgan, B. W., Wilson, S. R., Jones, N. B., and Edwards, D. P.: Trace gas emissions from savanna fires in Northern Australia, *J. Geophys. Res.*, 115, D16314, doi:10.1029/2009JD013309, 2010.
- Paulot, F., Wunch, D., Crounse, J. D., Toon, G. C., Millet, D. B., DeCarlo, P. F., Vigouroux, C., Deutscher, N. M., González Abad, G., Notholt, J., Warneke, T., Hannigan, J. W., Warneke, C., de Gouw, J. A., Dunlea, E. J., De Mazière, M., Griffith, D. W. T., Bernath, P., Jimenez, J. L., and Wennberg, P. O.: Importance of secondary sources in the atmospheric budgets of formic and acetic acids, *Atmos. Chem. Phys.*, 11, 1989–2013, doi:10.5194/acp-11-1989-2011, 2011.
- Perrin, A. and Vander Auwera, J.: An improved database for the 9 micron region of the formic acid spectrum, *J. Quant. Spectrosc. Ra.*, 108, 363–370, 2007.
- Perrin, A., Jacquemart, D., Kwabia Tchana, F., and Lacombe, N.: Absolute line intensities and new line lists for the 5.7 and 3.6 μm bands of formaldehyde, *J. Quant. Spectrosc. Ra.*, 110, 700–716, doi:10.1016/j.jqsrt.2010.02.004, 2009.
- Petersen, A. K., Warneke, T., Lawrence, M. G., Notholt, J., and Schrems, O.: First ground-based FTIR observations of the seasonal variation of carbon monoxide in the tropics, *Geophys. Res. Lett.*, 35, L03813, doi:10.1029/2007GL031393, 2008.
- Pougatchev, N. S., Connor, B. J., and Rinsland, C. P.: Infrared measurements of the ozone vertical distribution above Kitt Peak, *J. Geophys. Res.*, 100, 16689–16697, 1995.
- Quinn, P. K., Shaw, G., Andrews, E., Dutton, E. G., Ruoho-Airola, T., and Gong, S. L.: Arctic Haze: Current trends and knowledge gaps, *Tellus B*, 59, 99–114, doi:10.1111/j.1600-0889.2006.00238.x, 2007.
- Quinn, P. K., Bates, T. S., Baum, E., Doubleday, N., Fiore, A. M., Flanner, M., Fridlind, A., Garrett, T. J., Koch, D., Menon, S., Shindell, D., Stohl, A., and Warren, S. G.: Short-lived pollutants in the Arctic: their climate impact and possible mitigation strategies, *Atmos. Chem. Phys.*, 8, 1723–1735, doi:10.5194/acp-8-1723-2008, 2008.

- Razavi, A., Karagulian, F., Clarisse, L., Hurtmans, D., Coheur, P. F., Clerbaux, C., Müller, J. F., and Stavrou, T.: Global distributions of methanol and formic acid retrieved for the first time from the IASI/MetOp thermal infrared sounder, *Atmos. Chem. Phys.*, 11, 857–872, doi:10.5194/acp-11-857-2011, 2011.
- Rinke, A., Dethloff, K., and Fortmann, M.: Regional climate effects of Arctic Haze, *Geophys. Res. Lett.*, 31, L16202, doi:10.1029/2004GL020318, 2004.
- Rinsland, C. P., Jones, N. B., Connor, B. J., Logan, J. A., Pougatchev, N. S., Goldman, A., Murcray, F. J., Stephen, T. M., Pine, A. S., Zander, R., Mahieu, E., and Demoulin, P.: Northern and southern hemisphere ground-based infrared spectroscopic measurements of tropospheric carbon monoxide and ethane, *J. Geophys. Res.*, 103, 28197–28217, doi:10.1029/98JD02515, 1998.
- Rinsland, C. P., Goldman, A., Murcray, F. J., Stephen, T. M., Pougatchev, N. S., Fishman, J., David, S. J., Blatherwick, R. D., Novelli, P. C., Jones, N. B., and Connor, B. J.: Infrared solar spectroscopic measurements of free tropospheric CO, C₂H₆, and HCN above Mauna Loa, Hawaii: Seasonal variations and evidence for enhanced emissions from the southeast Asian tropical fires of 1997–1998, *J. Geophys. Res.*, 104, 18667–18680, doi:10.1029/1999JD900366, 1999.
- Rinsland, C. P., Mahieu, E., Zander, R., Demoulin, P., Forrer, J., and Buchmann, B.: Free tropospheric CO, C₂H₆, and HCN above center Europe: Recent measurements from the Jungfraujoch station including the detection of elevated columns during 1998, *J. Geophys. Res.*, 105, 24235–24249, doi:10.1029/2000JD900371, 2000.
- Rinsland, C. P., Meier, A., Griffith, D. W. T., and Chiou, L. S.: Ground-based measurements of tropospheric CO, C₂H₆, and HCN from Australia at 34° S latitude during 1997–1998, *J. Geophys. Res.*, 106, 20913–20924, doi:10.1029/2000JD000318, 2001.
- Rinsland, C. P., Jones, N. B., Connor, B. J., Wood, S. W., Goldman, A., Stephen, T. M., Murcray, F. J., Chiou, L. S., Zander, R., and Mahieu, E.: Multiyear infrared solar spectroscopic measurements of HCN, CO, C₂H₆, and C₂H₂ tropospheric columns above Lauder, New Zealand (45° S latitude), *J. Geophys. Res.*, 107, 4185, doi:10.1029/2001JD001150, 2002.
- Rinsland, C. P., Mahieu, E., Zander, R., Goldman, A., Wood, S., and Chiou, L.: Free tropospheric measurements of formic acid (HCOOH) from infrared ground-based solar absorption spectra: retrieval approach, evidence for a seasonal cycle, and comparison with model calculations, *J. Geophys. Res.*, 109, D18308, doi:10.1029/2004JD004917, 2004.
- Rinsland, C., Dufour, G., Boone, C., Bernath, P., Chiou, L., Coheur, P., Turquety, S., and Clerbaux, C.: Satellite boreal measurements over Alaska and Canada during June–July 2004: Simultaneous measurements of upper tropospheric CO, C₂H₆, HCN, CH₃Cl, CH₄, C₂H₂, CH₃OH, HCOOH, OCS, and SF₆ mixing ratios, *Global Biogeochem. Cy.*, 21, GB3008, doi:10.1029/2006GB002795, 2007.
- Rinsland, C. P., Mahieu, E., Chiou, L., and Herbin, H.: First ground-based infrared solar absorption measurements of free tropospheric methanol (CH₃OH): multidecade infrared time series from Kitt Peak (31.9° N 111.6° W): trend, seasonal cycle, and comparison with previous measurements, *J. Geophys. Res.*, 114, D04309, doi:10.1029/2008JD011003, 2009.
- Rodgers, C. D.: Inverse Methods for Atmospheric Sounding Theory and Practise, in: *Series on Atmospheric, Oceanic and Planetary Physics*, Vol. 2, World Scientific, Singapore, 2000.
- Rodgers, C. D. and Connor, B. J.: Intercomparison of remote sounding instruments, *J. Geophys. Res.*, 108, 4116, doi:10.1029/2002JD002299, 2003.
- Rothman, L. S., Gordon, I. E., Barbe, A., Benner, D. C., Bernath, P. F., Birk, M., Boudon, V., Brown, L. R., Campargue, A., Champion, J.-P., Chance, K., Coudert, L. H., Danaj, V., Devi, V. M., Fally, S., Flaud, J.-M., Gamache, R. R., Goldman, A., Jacquemart, D., Kleiner, I., Lacome, N., Lafferty, W. J., Mandin, J.-Y., Massie, S. T., Mikhailenko, S. N., Miller, C. E., Moazzen-Ahmadi, N., Naumenko, O. V., Nikitin, A. V., Orphal, J., Perevalov, V. I., Perrin, A., Predoi-Cross, A., Rinsland, C. P., Rotger, M., Simeckova, M., Smith, M. A. H., Sung, K., Tashkun, S. A., Tennyson, J., Toth, R. A., Vandaele, A. C., and Vander Auwera, J.: The Hitran 2008 molecular spectroscopic database, *J. Quant. Spectrosc. Ra.*, 110, 533–572, doi:10.1016/j.jqsrt.2009.02.013, 2009.
- Rudolph, J.: The tropospheric distribution and budget of ethane, *J. Geophys. Res.*, 100, 11369–11381, doi:10.1029/95JD00693, 1995.
- Sassi, F., Garcia, R. R., Boville, B. A., and Liu, H.: On temperature inversions and the mesospheric surf zone, *J. Geophys. Res.*, 107, 4380, doi:10.1029/2001JD001525, 2002.
- Schoeberl, M. R., Lait, L. R., Newman, P. A., and Rosenfield, J. E.: The structure of the polar vortex, *J. Geophys. Res.*, 97, 7859–7882, doi:10.1029/91JD02168, 1992.
- Shaw, G. E.: The Arctic Haze Phenomenon, *B. Am. Meteorol. Soc.*, 76, 2403–2413, doi:10.1175/1520-0477(1995)076<2403:TAHP>2.0.CO;2, 1995.
- Shindell, D. T., Chin, M., Dentener, F., Doherty, R. M., Faluvegi, G., Fiore, A. M., Hess, P., Koch, D. M., MacKenzie, I. A., Sander-son, M. G., Schultz, M. G., Schulz, M., Stevenson, D. S., Teich, H., Textor, C., Wild, O., Bergmann, D. J., Bey, I., Bian, H., Cuvelier, C., Duncan, B. N., Folberth, G., Horowitz, L. W., Jonson, J., Kaminski, J. W., Marmer, E., Park, R., Pringle, K. J., Schroeder, S., Szopa, S., Takemura, T., Zeng, G., Keating, T. J., and Zuber, A.: A multi-model assessment of pollution transport to the Arctic, *Atmos. Chem. Phys.*, 8, 5353–5372, doi:10.5194/acp-8-5353-2008, 2008.
- Simpson, I. J., Akagi, S. K., Barletta, B., Blake, N. J., Choi, Y., Diskin, G. S., Fried, A., Fuelberg, H. E., Meinardi, S., Rowland, F. S., Vay, S. A., Weinheimer, A. J., Wennberg, P. O., Wiebring, P., Wisthaler, A., Yang, M., Yokelson, R. J., and Blake, D. R.: Boreal forest fire emissions in fresh Canadian smoke plumes: C₁–C₁₀ volatile organic compounds (VOCs), CO₂, CO, NO₂, NO, HCN and CH₃CN, *Atmos. Chem. Phys.*, 11, 6445–6463, doi:10.5194/acp-11-6445-2011, 2011.
- Singh, H. B. and Zimmerman, P.: Atmospheric distribution and sources of nonmethane hydrocarbons, in: *Gaseous Pollutants: Characterization and Cycling*, edited by: Nriagu, J. O., John Wiley & Sons, New York, NY, USA, 177–225, 1992.
- Stavrakou, T., Müller, J.-F., De Smedt, I., Van Roozendaal, M., van der Werf, G. R., Giglio, L., and Guenther, A.: Evaluating the performance of pyrogenic and biogenic emission inventories against one decade of space-based formaldehyde columns, *Atmos. Chem. Phys.*, 9, 1037–1060, doi:10.5194/acp-9-1037-2009, 2009.

- Stavrakou, T., Guenther, A., Razavi, A., Clarisse, L., Clerbaux, C., Coheur, P.-F., Hurtmans, D., Karagulian, F., De Mazière, M., Vigouroux, C., Amelynck, C., Schoon, N., Laffineur, Q., Heinesch, B., Aubinet, M., Rinsland, C., and Müller, J.-F.: First space-based derivation of the global atmospheric methanol emission fluxes, *Atmos. Chem. Phys.*, 11, 4873–4898, doi:10.5194/acp-11-4873-2011, 2011.
- Stavrakou, T., Muller, J.-F., Peeters, J., Razavi, A., Clarisse, L., Clerbaux, C., Coheur, P.-F., Hurtmans, D., De Mazière, M., Vigouroux, C., Deutscher, N. M., Griffith, D. W. T., Jones, N., and Paton-Walsh, C.: Satellite evidence for a large source of formic acid from boreal and tropical forests, *Nat. Geosci.*, 5, 26–30, doi:10.1038/ngeo1354, 2012.
- Stohl, A.: Characteristics of atmospheric transport into the Arctic troposphere, *J. Geophys. Res.*, 111, D11306, doi:10.1029/2005JD006888, 2006.
- Sussmann, R. and Borsdorff, T.: Technical Note: Interference errors in infrared remote sounding of the atmosphere, *Atmos. Chem. Phys.*, 7, 3537–3557, doi:10.5194/acp-7-3537-2007, 2007.
- Sussmann, R., Forster, F., Rettinger, M., and Jones, N.: Strategy for high-accuracy-and-precision retrieval of atmospheric methane from the mid-infrared FTIR network, *Atmos. Meas. Tech.*, 4, 1943–1964, doi:10.5194/amt-4-1943-2011, 2011.
- Tereszczuk, K. A., González Abad, G., Clerbaux, C., Hurtmans, D., Coheur, P.-F., and Bernath, P. F.: ACE-FTS measurements of trace species in the characterization of biomass burning plumes, *Atmos. Chem. Phys.*, 11, 12169–12179, doi:10.5194/acp-11-12169-2011, 2011.
- Tereszczuk, K. A., González Abad, G., Clerbaux, C., Hadji-Lazaro, J., Hurtmans, D., Coheur, P.-F., and Bernath, P. F.: ACE-FTS observations of pyrogenic trace species in boreal biomass burning plumes during BORTAS, *Atmos. Chem. Phys.*, 13, 4529–4541, doi:10.5194/acp-13-4529-2013, 2013.
- Toon, G. C., Blavier, J.-F., Sen, B., Margitan, J. J., Webster, C. R., May, R. D., Fahey, D. W., Gao, R., Del Negro, L., Proffitt, M., Elkins, J., Romashkin, P. A., Hurst, D. F., Oltmans, S., Atlas, E., Schauffler, S., Flocke, F., Bui, T. P., Stimpfle, R. M., Bonne, G. P., Voss, P. B., and Cohen, R. C.: Comparison of MkIV balloon and ER-2 aircraft profiles of atmospheric trace gases, *J. Geophys. Res.*, 104, 26779–26790, doi:10.1029/1999JD900379, 1999.
- Trenberth, K. E., Jones, P. D., Ambenje, P., Bojariu, R., Easterling, D., Klein Tank, A., Parker, D., Rahimzadeh, F., Renwick, J. A., Rusticucci, M., Soden, B., and Zhai, P.: Observations: Surface and Atmospheric Climate Change, in: *Climate Change 2007: The Physical Science Basis. Contribution of Working Group I to the Fourth Assessment Report of the Intergovernmental Panel on Climate Change*, edited by: Solomon, S., Qin, D., Manning, M., Chen, Z., Marquis, M., Averyt, K. B., Tignor, M., and Miller, H. L., Cambridge University Press, Cambridge, UK and New York, NY, USA, 2007.
- Viatte, C., Strong, K., Paton-Walsh, C., Mendonca, J., O'Neill, N. T., and Drummond, J. R.: Measurements of CO, HCN, and C₂H₆ total columns in smoke plumes transported from the 2010 Russian boreal forest fires to the Canadian high Arctic, *Atmosphere-Ocean*, 51, 1–10, doi:10.1080/07055900.2013.823373, 2013.
- Vigouroux, C., Hendrick, F., Stavrakou, T., Dils, B., De Smedt, I., Hermans, C., Merlaud, A., Scolas, F., Senten, C., Vanhaelewyn, G., Fally, S., Carleer, M., Metzger, J.-M., Müller, J.-F., Van Roozendael, M., and De Mazière, M.: Ground-based FTIR and MAX-DOAS observations of formaldehyde at Réunion Island and comparisons with satellite and model data, *Atmos. Chem. Phys.*, 9, 9523–9544, doi:10.5194/acp-9-9523-2009, 2009.
- Vigouroux, C., Stavrakou, T., Whaley, C., Dils, B., Duflot, V., Hermans, C., Kumps, N., Metzger, J.-M., Scolas, F., Vanhaelewyn, G., Müller, J.-F., Jones, D. B. A., Li, Q., and De Mazière, M.: FTIR time-series of biomass burning products (HCN, C₂H₆, C₂H₂, CH₃OH, and HCOOH) at Reunion Island (21° S, 55° E) and comparisons with model data, *Atmos. Chem. Phys.*, 12, 10367–10385, doi:10.5194/acp-12-10367-2012, 2012.
- Von Kuhlmann, R., Lawrence, G., Crutzen, P. J., and Rasch, P. J.: A model for studies of tropospheric ozone and nonmethane hydrocarbons: model evaluation of ozone-related species, *J. Geophys. Res.*, 108, 4729, doi:10.1029/2002JD003348, 2003.
- Wagner, T., Beirle, S., Grzegorski, M., and Platt, U.: Global trends (1996–2003) of total column precipitable water observed by Global Ozone Monitoring Experiment (GOME) on ERS-2 and their relation to near-surface temperature, *J. Geophys. Res.*, 111, D12102, doi:10.1029/2005JD006523, 2006.
- Warneck, P.: Chemistry of the natural atmosphere, in: *International Geophysics*, Vol. 71, 2nd Edn., Academic Press, San Diego, 2000.
- Xiao, Y., Jacob, D. J., and Turquety, S.: Atmospheric acetylene and its relationship with CO as an indicator of air mass age, *J. Geophys. Res.*, 112, D12305, doi:10.1029/2006JD008268, 2007.
- Xiao, Y., Logan, J. A., Jacob, D. J., Hudman, R. C., Yantosca, R., and Blake, D. R.: Global budget of ethane and regional constraints on US sources, *J. Geophys. Res.*, 113, D21306, doi:10.1029/2007JD009415, 2008.
- Zander, R., Duchatelet, P., Mahieu, E., Demoulin, P., Roland, G., Servais, C., Auwera, J. V., Perrin, A., Rinsland, C. P., and Crutzen, P. J.: Formic acid above the Jungfraujoch during 1985–2007: observed variability, seasonality, but no long-term background evolution, *Atmos. Chem. Phys.*, 10, 10047–10065, doi:10.5194/acp-10-10047-2010, 2010.
- Zeng, G., Wood, S. W., Morgenstern, O., Jones, N. B., Robinson, J., and Smale, D.: Trends and variations in CO, C₂H₆, and HCN in the Southern Hemisphere point to the declining anthropogenic emissions of CO and C₂H₆, *Atmos. Chem. Phys.*, 12, 7543–7555, doi:10.5194/acp-12-7543-2012, 2012.
- Zhao, Y., Strong, K., Kondo, Y., Koike, M., Matsumi, Y., Irie, H., Rinsland, C. P., Jones, N. B., Suzuki, K., Nakajima, H., Nakane, H., and Murata, I.: Spectroscopic measurements of tropospheric CO, C₂H₆, C₂H₂, and HCN in northern Japan, *J. Geophys. Res.*, 107, 4343, doi:10.1029/2001JD000748, 2002.